Design and Analysis of Liquid Rocket Engine Regenerative Cooling Jackets: *Emphasis on Computational Modeling*

By

Nicholas Costanzo McGuire
B.S. (University of California, Davis) 2007

THESIS

Submitted in partial satisfaction of the requirements for the degree of

MASTER OF SCIENCE

in

Mechanical and Aeronautical Engineering

in the

OFFICE OF GRADUATE STUDIES

of the

UNIVERSITY OF CALIFORNIA

DAVIS

Approved:

Dr. Roger Davis

Dr. Jean-Pierre Delplanque

Dr. Daniel Noren

Committee in Charge

2009

Abstract

An analytical computational procedure was developed in MATLAB to efficiently design the coolant channel height profile of a regeneratively cooled liquid rocket engine using the chamber wall temperature as the primary design point. The procedure employs a linear control volume marching scheme proceeding from the coolant channel inlet up through the chamber wall to the main injector face, successively iterating on the primary fluid variables. A conjugate analysis is used to accurately capture the heat transfer interaction between the hot combustion gases in the chamber and the cryogenic liquid fuel in the coolant passages. Verification of the procedure was achieved by comparing analytical results with exact solutions and another existing fluid analysis procedure in addition to published experimental data from the RL10 engine. A design trade study focusing on the main descent engine for the Altair Lunar Lander was carried out to explore the coolant channel design capabilities of the procedure at varying chamber pressures and mixture ratios as well using different chamber materials. The results of this trade study pointed to lower pressures and moderate mixture ratios as providing the best results. A copper chamber, as opposed to a stainless steel chamber, also resulted in beneficial lower pressure losses and slightly higher levels of heat pickup in the coolant channels in several cases. Overall, the procedure was successful in both designing coolant channel height profiles and in analyzing existing channels in an accurate and timely fashion while maintaining a sufficient level of flexibility and expansion capabilities.

Table of Contents

Acknowledgments

I would like to offer extensive thanks to Dr. Bryan Campbell of Aerojet for the many hours he spent helping me with the technical side of this project and providing me with the necessary tools and data to complete it. I would also like to thank Todd Neill of Aerojet for creating the opportunity to work on this research in conjunction with Aerojet. Finally I would like to thank Dr. Roger Davis, my thesis advisor, for the countless hours of support and assistance he has provided me with my thesis over the last two years as his graduate student.

Nomenclature

A = coolant channel cross-sectional area
A_{fin} = fin convective surface area
A_p = coolant channel perimeter
AR = aspect ratio
a = speed of sound
C_p = specific heat at constant pressure
D = diameter
dx = control volume length
E = modulus of elasticity
f = friction coefficient
g_c = gravitational correction factor
H = static enthalpy
h = heat transfer coefficient
hgt = height
I_{sp} = specific impulse
i = position index
k = thermal conductivity
L = total coolant channel path length
M = Mach number
MW = molar weight
$\dot{m}$ = mass flow rate
m = intermediate calculation parameter
N = number of X
P = static pressure
Pc = chamber pressure
Pr = Prandtl number
$\dot{Q}$ = heat transfer rate
q'' = heat flux
Re = Reynolds number
R_u = universal gas constant
S = source term
T = static temperature
t = wall thickness
u = velocity
V = velocity
w = width
α = thermal expansion coefficient
α_c = fuel film cooling flow angle
ε = roughness
γ = specific heat ratio
η = efficiency
ρ = density
μ = dynamic viscosity

Subscripts:

avg = average
c = fuel film cooling
cool = bulk coolant or coolant channel(s)
cv = control volume(s)
cw = cold wall
f = film
fin = coolant channel fin/land
g = free stream combustion gas or chamber
hw = hot wall
hyd = hydraulic
i = inlet
m = metal
r = reference property
sm = surface
t = total
throat = combustion chamber throat

List of Figures

List of Tables

1. Introduction

One of the most important aspects that must be considered when designing a new liquid-fueled rocket engine is how to effectively cool the chamber and nozzle. Some manner of cooling is imperative to prevent their deterioration or complete destruction due to the intense heat to which both are subjected. The typical methods of cooling often include one or even a combination of the following methods: regenerative, dump, film, transpiration, ablative and radiation cooling.[12] The method that is the primary focus of this current effort is regenerative cooling, which is by far one of the most commonly used methods to cool moderate thrust range engines. Regenerative cooling works by passing the cryogenic fuel through channels or tubes built into the wall of the thrust chamber and/or nozzle. This effectively cools the wall by exchanging the heat generated by the combustion gases with the colder fuel before it enters the combustion chamber through the main injector. Experiments performed in the past have attempted to use the cryogenic liquid oxidizer instead of the fuel as the coolant but this was not examined in this study. A cross-section of a sample regeneratively cooled wall that uses longitudinal channels is shown below in Figure 1.1:

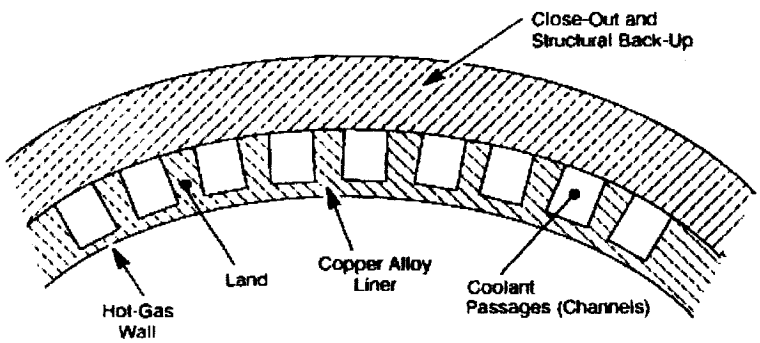

Figure 1.1. Regeneratively cooled chamber wall cross-section[12]

There are many different types and configurations of regenerative cooling including channels or tubes that spiral around the nozzle or loop up and down its length. However, longitudinal channels, running in a single pass axially along the outer wall as shown in Figure 1.1, is the primary type considered for this study. In addition to regenerative cooling, fuel film cooling is also sometimes used to supplement regenerative cooling when specific fuels are used, such as RP-1 and methane. Fuel film cooling works by injecting a small percentage of the cryogenic fuel coolant through tiny orifices in the chamber wall at various axial locations along the thrust chamber; this provides a cool film boundary layer between the wall and the hotter free-stream combustion gases. This boundary layer helps keep the wall cooler and reduces the amount of heat absorbed by the bulk coolant flow. Fuel film cooling was initially researched in this study but was not included in the final procedure due to the added level of complexity it requires.

1.1. Development Motivations and Goals

The primary motivation behind this thesis is to develop a design and analysis procedure for rocket engine combustion chamber cooling channels. A previously developed design tool, written in Simulink and Matlab, simulates the engine, allows trade studies to be performed, and serves as a primary source of technical data. In order to run an engine simulation with this procedure, data from thermal analysts must be obtained to provide the sections of the procedure related to heat transfer with the necessary inputs. This adds a significant amount of time to the process of running the simulation since the analysts must separately rerun analytical tools each time a new case needs to be run. The reason for developing this procedure is to eliminate the need for consulting the thermal analysts by providing a stand alone procedure that correctly sizes the longitudinal coolant

channels of a regenerative-cooled liquid rocket engine, given basic inlet conditions and geometry, in order to maintain a constant prescribed chamber wall temperature. Its secondary function is to analyze a pre-existing coolant channel geometry profile, and based on prescribed inlet conditions, calculate and output all of the important fluid properties and temperature profiles along the length of the channel. A primary factor in the procedure's practicality is its ability to save time and thus it must quickly provide results that are accurate enough to support trade studies as well as preliminary design and analysis work.

An important first step that must be taken when discussing this procedure is to layout the primary attributes that define its usefulness and how the combination of these features lead to a unique solution to this problem. One of the prime benefits of this procedure is its development in MATLAB, one of the most widely used engineering-oriented computer languages, both in the workplace and at educational institutions. The fact that it was written in MATLAB also means that it can be seamlessly integrated with Simulink, an extremely powerful block diagram style modeling and simulation program, which is currently being used to simulate various rocket engines.

Another critical aspect of the new procedure is that it employs a conjugate design and analysis technique, combining both fluid dynamics and heat transfer in order to accurately model the thermal interaction between the combustion chamber gases and the liquid fuel coolant. In addition, in order to increase the accuracy of these calculations, viscous friction in the channels is taken into account through the use of the Churchill correlation[6] which allows the usage of different values for the channels surface roughness to capture the different manufacturing tolerances used in channel fabrication if

desired. Similarly, real fluid properties were used throughout the procedure instead of making isentropic or ideal fluid assumptions, again to enhance accuracy. Especially when dealing with the high temperatures and pressures and unusual fluids used in liquid rocket engines, it is imperative that real fluids properties are used as extensively as possible since most of the ideal assumptions are not valid in the flow regimes under consideration. Currently the program RefProp[18], developed by NIST, is used to lookup the coolants various fluid properties and at this time, it supports oxygen, parahydrogen, hydrogen, methane, nitrogen, helium, RP-1 and water. Thus, the procedure can theoretically support any number of these propellants. The only limitation at this point is that RefProp cannot be used to obtain real fluid data for the combustion gases in the chamber which require a separate set of look-up tables. As long as these tables are available or can be generated to support the user's choice of fuel and oxidizer, all of the RefProp fuels may be used and the procedure can support all of the common propellant choices.

One of the most important attributes of the procedure is its ability to optimize the coolant channel geometry when running in design mode. When designing a coolant channel profile, the inlet conditions, including the height of the inlet to the channel and the desired hot wall temperature that needs to be maintained along the length of the chamber, are initially specified. With this information, the procedure will attempt to design a coolant channel profile by varying the height of the channel along the length of the chamber until it achieves a profile that maintains the constant desired hot wall temperature.

The final two assets that the procedure employs that increase its usefulness are its ability to support multiple metal layers or thermal coatings in the chamber wall and the built in structural analysis and fabrication limits. The chamber wall of a rocket engine is sometimes very complex from a materials standpoint, with multiple layers of different metals bonded together and/or thin thermal coatings that prevent the high temperature and corrosive combustion gases from melting or eating away at the surface of the wall. At this current stage of development, the procedure allows the user to input up to three different layers of metals or coatings with varying degrees of thickness. The procedure currently supports four different materials including stainless steel, copper, zirconium oxide, and NARloy-Z, but is setup to allow more materials to be added if data correlating thermal conductivity as a function of material temperature is available. It would be advantageous to expand this section of the procedure to a theoretically infinite number of layers but this requires significant effort beyond the scope of this investigation given that its focus is on the conjugate heat transfer and not the wall structure. By allowing multiple layers and types of materials in the chamber wall, more realistic chambers can be designed and chambers already in existence that use a wide array of materials can still be analyzed successfully.

Finally, in regards to structural analysis, as part of the normal analysis or design process, the procedure has a section that performs a simple flat surface in bending calculation to verify that the pressure forces within the coolant channel are not high enough to deform or lead to the failure of the coolant channel wall. A simple thermal stress analysis is also performed as well. Since these types of calculations are approximate, a more detailed structural analysis would need to be conducted if the

pressure forces or thermal stresses turn out to be too high. In addition, there are built in checks at the beginning of the procedure that limit various geometric parameters in the engine to remain within today's known fabrication limits or the fabrication limits of the facilities that would be used to manufacture the engine's thrust chamber.

1.2. Background

The topic of coolant channel design has been the focus of research for some time now although the development of rectangular longitudinal coolant channels has become more common recently since the manufacturing techniques required to construct them with exceptional accuracy are relatively newer. The original form of longitudinal cooling, which is not directly addressed by this investigation, was typically achieved using a series of tubes brazed together along the inside wall of the chamber to form coolant passageways. Modern coolant channels are usually integrated into the wall material and fabricated with advanced machining and etching processes.

One of the early studies undertaken to look at issues surrounding coolant channels in regeneratively cooled engines was performed by NASA in the mid-1960s at the Lewis Research Center[16]. In conjunction with hot-fire tests and studies performed with real hardware, a computer program was also developed that incorporated finite-difference numerical techniques in order to obtain and characterize wall temperature and heat flux distributions in chambers with rectangular coolant channels. Their analyses were carried out at steady-state and focused primarily on the various heat transfer coefficients, their variation across a given coolant channel, and the effects they had on the wall temperatures. Although their heat transfer analysis of the coolant channels was very detailed to obtain these results, their work focused primarily on the analysis of given

channel geometry and experimental data. This allowed the researchers to concentrate on the trends of the heat transfer coefficients and their effects. Thus, although they have provided a solid foundation for coolant channel analysis in their specific case, which used hydrogen and fluorine, their technical note did not document any attempt to use or develop their procedure for coolant channel design purposes.

One of the definitive books on the design of liquid-propellant rocket engines, first written by Huzel and Huang[12] in the mid-1960s, before being updated several times since then through the early 1990s, discusses regenerative cooling in some detail. The first edition from 1967 outlines regenerative cooling, focusing primarily on tubular wall construction and the associated brazing techniques involved in its construction. Rectangular coolant channels, however, were not mentioned although a section has since been added and appears in the newest edition written in 1992. The research they present highlights the importance and benefits of channel-wall design in high pressure applications as well as in high heat-flux situations. In the newest edition, several computer programs are mentioned including a boundary-layer program that is used to compute heat transfer coefficients as well as several programs that are used to analyze a given configuration and solve for the important temperature distributions in the chamber wall. One such program, called REGEN, performs a two-dimensional analysis while coupled with one-dimensional equations for compressible flow. Again, no specific mention is made about using any of the procedures in a design specific fashion and instead, focus primarily on analyzing the performance of given geometry rather than attempting to output a new computer-generated geometry.

Another important paper from which many of the equations and methodology used in the development of the current procedure come is the NASA Technical Memorandum on the RL10A rocket engine written in 1997[2]. An extensive overview is given that outlines the primary equations used to develop a heat transfer model that accurately simulates the interaction between the hot combustion gases and the cryogenic fuel flowing through the coolant tubes. Several existing procedures were used in the analysis performed including the Rocket Thermal Evaluation (RTE) procedure, the RL10 ROCETS system model, and another thermal analysis procedure developed at the NASA Lewis Research Center. Given that the RL10A engine was developed in the 1960s, their research was performed and procedure was developed to enhance the understanding of the existing RL10 engine. This also provided validation of these analysis tools for use on future engines for which there is no existing data. Once again, the primary use of these various system models and analysis procedure was to develop a further understanding of the intricacies of the RL10A engine in the hopes of improving its performance and thus, it was not used to specifically design new coolant channels for the engine. The RL10 engine uses coolant tubes rather than rectangular channels to perform its regenerative cooling; therefore, although a perfect comparison of results from their research can not be compared to this project, general validation is possible because the equations and methodology overlap between the two studies.

In a similar NASA Technical Memorandum[23] written a year later, the use of high aspect ratio coolant channels was considered in several different design configurations including several continuously variable designs, a bifurcated design, and finally, two stepped channel wall designs. In order to analyze these designs, two programs, the rocket

thermal evaluation procedure (RTE) and a nozzle analysis procedure (TDK), were coupled and used in tandem to solve for the hot wall temperature and coolant pressure drops along the channels. With the completion of the study and after taking fabrication limitations into account, it was determined that the high aspect ratio bifurcated channel design was the most beneficial although the other designs provided very promising results as well. Bifurcated channels however are beyond the scope of this current study. If the channel widths are defined small enough though in a continuous channel wall design, it is very likely that this procedure will generate a profile with higher aspect ratio channels in order to compensate for the loss of channel width.

Some of the most recent research completed on regenerative cooling jacket design was performed by several graduate students at Purdue University in 2006[21] in order to study performance benefits of different coolant channel geometries and chamber conditions. Their primary focus was on performing parametric studies of channel geometry, chamber pressures, aspect ratios, channel widths and the number of channels for a LOX/methane engine developed for the NASA Crew Exploration Vehicle. Their results indicate that a stepped channel configuration in which the cross-section of the coolant channel changes at several distinct axial locations outperforms a constant cross-section channel. This conclusion points to the fact that a channel whose cross-section is continuously varied may result in even greater performance increases, validating the development goals of the procedure developed and described here.

2. Design and Analysis Methods

In order to properly design or analyze the coolant flow path through a rocket engine, a linear marching scheme is used in the current effort to examine the entire length of a coolant channel. This method requires that the channels be broken up into a defined number of control volumes which is specified by the user to achieve the desired level of accuracy and fidelity. In both the design and analysis scenarios, all of the necessary fluid and thermal parameters at the inlet to the coolant channels must be specified. Guesses for the values of each of these parameters at the downstream end of the first control volume are then made. Three primary governing equations are subsequently used to update these downstream properties in an iterative fashion before the process repeats itself with each successive control volume until all control volumes have been solved.

2.1. Governing Equations and Correlations

The primary equations governing the fluid dynamics of the liquid coolant are the conservation of mass, momentum and energy equations. These equations form the backbone of the fluid analysis and provide solutions for several of the important downstream fluid properties. The conservation of mass in differential form and the update formula for the downstream mass flow rate are given in Eqs. (2.1) and (2.2):

$$\frac{\partial}{\partial x}(\rho u) = S_{fc} \tag{2.1}$$

$$\dot{m}^{i+1} = \dot{m}^{i} - \dot{m}_{c}^{i} \tag{2.2}$$

(Note: superscript "i" refers to the current control volume, not an exponent)

In the case where fuel film cooling is not applied, the source term (S_c) in equation 2.1 and the final term in equation 2.2 will go to zero in which case the formulas reduce to trivial single inlet and exit flow. Similarly, the conservation of momentum equation in conservative differential form as well as the update formula for the downstream static pressure are presented here in Eqs. (2.3) and (2.4):

$$\frac{\partial}{\partial x}(\rho u) = -\frac{\partial p}{\partial x} + \frac{\partial f}{\partial x} + S_c \tag{2.3}$$

$$P^{i+1} = \frac{\left(P^i\left(A^i + \frac{A^{i+1} - A^i}{2}\right) + P_c^i A_c^i \cos(\alpha_c) - \rho_{avg} f V_{avg}^2 A_p dx + \dot{m}^i V^i - \dot{m}^{i+1} V^{i+1} - \dot{m}_c^i V_c^i \cos(\alpha_c)\right)}{\left(A^{i+1} - \frac{A^{i+1} - A^i}{2}\right)} \tag{2.4}$$

Finally, the conservation of energy equations in conservative differential form and the update formula for the downstream static enthalpy are given in Eqs. (2.5) and (2.6):

$$\frac{\partial}{\partial x}(\rho u H) = \frac{\partial}{\partial x}\left(k\frac{\partial T}{\partial x}\right) + S_c \tag{2.5}$$

$$H^{i+1} = \frac{1}{\dot{m}^{i+1}}\left[\dot{Q}^i + \dot{m}^i\left(H^i + \frac{(\dot{m}^i)^2}{2(\rho^i)^2(A^i)^2}\right) + \dot{m}_c^i\left(H_c^i + \frac{(\dot{m}_c^i)^2}{2(\rho_c^i)^2(A_c^i)^2}\right)\right] - \frac{(\dot{m}^{i+1})^2}{2(\rho^{i+1})^2(A^{i+1})^2} \tag{2.6}$$

Both the conservation of momentum and energy equations, like the conservation of mass equation, include terms that account for fuel film cooling, when required. An important term that shows up in the momentum equation is the friction factor, f, which accounts for the viscous wall friction along the length of the coolant channel. This term is calculated using the Churchill correlation given in Eq. (2.7)[6]:

$$f = \left[\left(\frac{8}{\mathrm{Re}}\right)^{12} + \frac{1}{(A1 + B1)^{3/2}}\right]^{1/12}, \quad A1 = \left[2.457 \cdot \ln\left(\frac{1}{(7/\mathrm{Re})^{0.9} + 0.27(\varepsilon/D)}\right)\right]^{16}, \quad B1 = \left(\frac{37{,}530}{\mathrm{Re}}\right)^{16} \tag{2.7}$$

Another key term that shows up in the energy equation is the heat transfer rate, $\dot{Q}$, which accounts for the amount of heat transferred into the coolant from the combustion gas

every second. In order to understand where this heat transfer rate value comes from, the heat transfer interaction between the coolant channels and combustion gases must first be described and will be discussed further in section 2.5.

2.2. Boundary and Input Conditions

Given that a linear marching scheme is used to design or analyze the coolant channel flow path, the only boundary conditions that exist are those at the channel inlet manifold. The three primary fluid parameters pertaining to the bulk coolant that must be specified are the static temperature, the static pressure, and the inlet mass flow rate. In addition, several quantities must also be specified for the combustion gas flow through the rocket engine's chamber including the chamber mass flow rate, total pressure and temperature, and the mixture ratio. All but the chamber mass flow rate are stored as vector quantities to allow a greater degree of fidelity, as opposed to assuming they are constant, in case the user knows their values as a function of axial position in the chamber from test data or another modeling tool.

In addition to these fluid properties, numerous other parameters need to be specified before a design or analysis case can be run. These include the chamber hydraulic diameter, the chamber wall thickness, and the width of the coolant channels, all of which are again stored as vector quantities as a function of axial position along the chamber. At this point, initial guesses for the hot and cold side temperatures of the chamber wall must be made, in addition to specifying the desired tolerance to which variables are to be converged. Furthermore, the number and type of materials used in the chamber wall must also be stored along with each layer's thickness in a matrix to handle this information. Finally, the last several input conditions that must be provided vary

dependent on whether the procedure is running in design or analysis mode. In design mode, the total length of the coolant channel path must be specified along with the height of the inlet. In analysis mode however, a height profile along the entire length of the coolant channel must be provided along with its corresponding axial positions.

2.3. Numerical Constraints: Iteration and Design

In addition to the constraints imposed by the boundary and input conditions, there are several other areas in which the procedure is constrained. The two primary aspects of the procedure that are affected by these constraints are the iteration routines used throughout the procedure to obtain convergence and in the design routine responsible for optimizing the coolant channel height profile.

Beginning with the iteration routines, as each successive control volume is accessed while moving along the coolant channel, all of the fluid properties and parameters at the downstream exit of the control volume must reach convergence before proceeding to the next control volume. This action is of course mandated because the exit of the preceding control volume is the inlet to the next control volume. Given that only the inlet conditions of each control volume is known and the downstream properties are all unknown and dependent on each other, numerical iteration must be employed since a closed-form solution of the numerous equations does not exist. As a starting point, several of the downstream properties including the pressure, temperature, enthalpy, density and dynamic viscosity, are set equal to their corresponding upstream properties to provide an initial guess for iterating. These initial guesses allow all of the downstream fluid properties to be calculated before a residual is determined for each parameter. The residual in this case is simply the difference between the variable's current value and the

value from the previous iteration divided by the current value. This difference is then compared with the specified error tolerance, which, as with most engineering applications, is typically set to 1×10^{-5}, although a different tolerance may be specified given the accuracy required for a specific application. The iteration loop is constrained in such a way that it will not finish iterating until all of the residuals for the requisite fluid properties are less than the specified tolerance. A block diagram outline of this scheme is shown below in Figure 2.1:

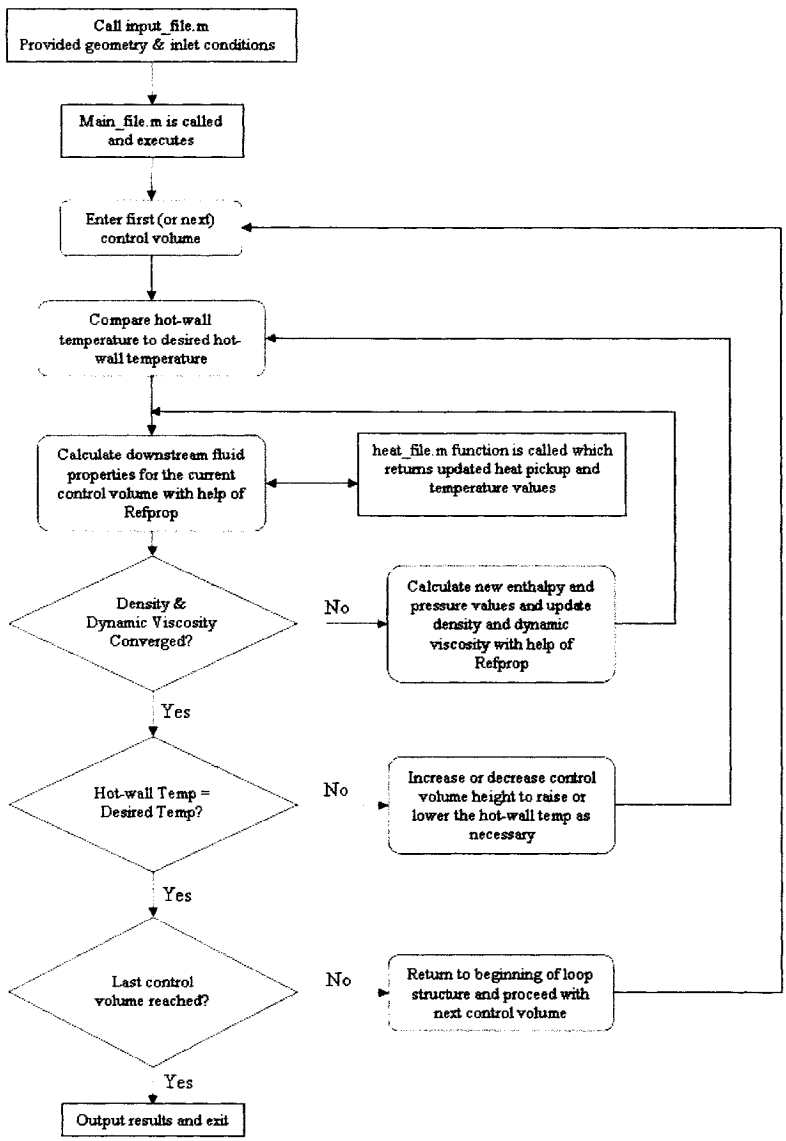

Figure 2.1. Procedure iteration routine

A virtually identical iteration scheme is used in the wall heat transfer routine (discussed later) because several of the necessary heat transfer variables are dependent on the chamber wall temperatures that are also unknown. Once again, this iteration loop will not finish until all of heat transfer variable residuals are less than the tolerance, which may be specified separately from the previously mentioned tolerance.

Similarly, an additional iteration routine is used in the coolant channel design routine which is constrained even further by three important physical boundaries. When the procedure is running in design mode, the coolant channel design routine is implemented after a control volume has converged to determine if the chamber's hot wall temperature is equal to the prescribed constant temperature within the specified tolerance. If the temperature is above the prescribed value, the routine reduces the coolant flow area by decreasing the height, which thereby increases the coolant velocity resulting in greater cooling. If the temperature is below the prescribed value, however, the height is increased which accomplishes the reverse and provides less wall cooling. Each time a change in height is made all of the fluid properties in the control volume must be recalculated and converged again using the previous iteration loop. A flow chart outlining this procedure is shown below in Figure 2.2:

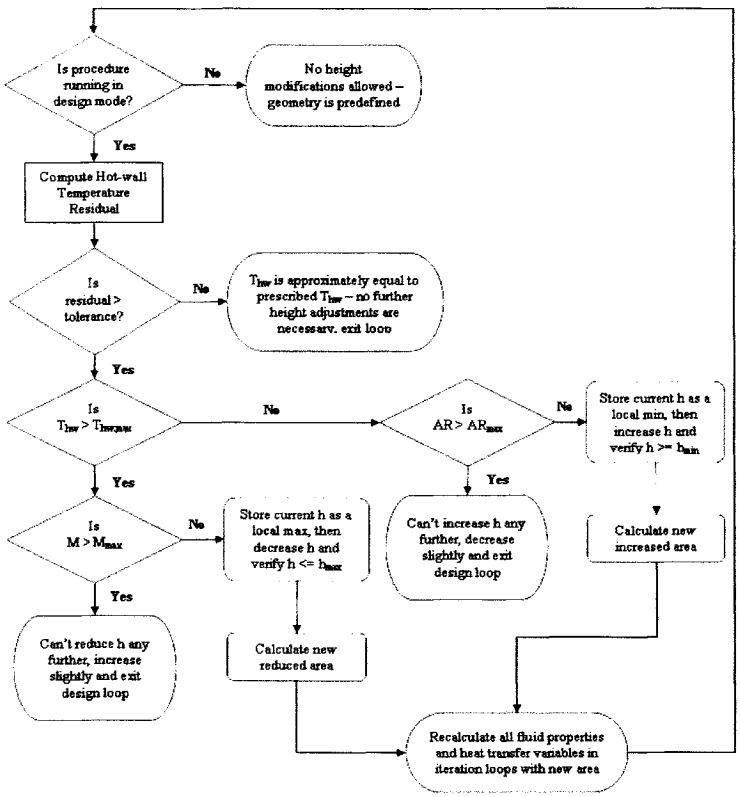

Figure 2.2. Design mode height modification routine

This coolant channel design routine iterates in the same fashion as this other inner iteration loop and will continue to modify the height until the hot wall temperature residual is less than the specified tolerance. The three additional physical constraints that govern this routine are limits on the amount the height can be changed in the form of a maximum Mach number, a maximum coolant channel aspect ratio and a maximum and minimum height. If the Mach number exceeds 0.3, the height can no longer be reduced any further since the area is becoming too small. If the coolant channel aspect ratio exceeds the specified maximum value (typically between 5 and 8) then the height can no longer be increased because the coolant channels are becoming too thin. Finally, no further height changes can be made if either the maximum or minimum height values (0.01 or 0.6 inches) are reached. If any of these constraints are reached, the design iteration scheme must terminate prematurely and the user will be forced to accept a hot

wall temperature that is not within the specified tolerance. In order to minimize the magnitude by which the temperature exceeds the maximum value, the routine jumps back to the last viable Mach number or aspect ratio below the limit when the upper or lower hot wall temperature limit is exceeded. The iteration algorithm takes much smaller step sizes, in terms of height modification, until the chosen height results in a Mach number or aspect ratio very close but just below the specified limits.

2.4. Design versus Analysis Strategy

As mentioned previously, the procedure is capable of running in either a design or analytical capacity. The final outputs of both simulations are very similar, although coolant channel height profile is outputted in design mode and not in analysis mode since it is an input parameter, the methods used to obtain the results are slightly different.

In design mode, the procedure takes the inlet conditions and as discussed before, marches linearly through each of the control volumes, converging each one serially, modifying their heights in order to achieve the desired hot wall temperature. Two nested iteration loops are required to achieve a solution: the innermost loop that converges the fluid variables in each control volume, and an outer iteration loop that modifies the cooling channel height and forces the procedure to re-run the innermost iteration loop to obtain new updated fluid property values with the new height.

Likewise, in analysis mode the procedure proceeds in virtually the same fashion except for the fact that the input condition variables are slightly different as mentioned before. In addition, since the height profile is already known, the outermost iteration loop and the height modification routine is bypassed since no further geometry modifications are required once the downstream parameters in the control volume have

been determined within the innermost iteration loop. The bypassing of this additional iteration loop and modification scheme obviously results in greatly reduced solution times.

2.5. Heat Transfer Equations and Methodology

One of the most important aspects of analyzing the coolant channels is accurately capturing the heat transfer interaction that takes place between the hot combustion gases flowing through the chamber and the liquid fuel coolant in the channels. This interaction is broken up into three different thermal regimes: the convective hot gas side, the conduction through the chamber wall, and the convective cold gas or coolant side. The schematic in Figure 2.3 below shows a typical cross-section of a regeneratively cooled rocket engine chamber where each of these three regimes exist:

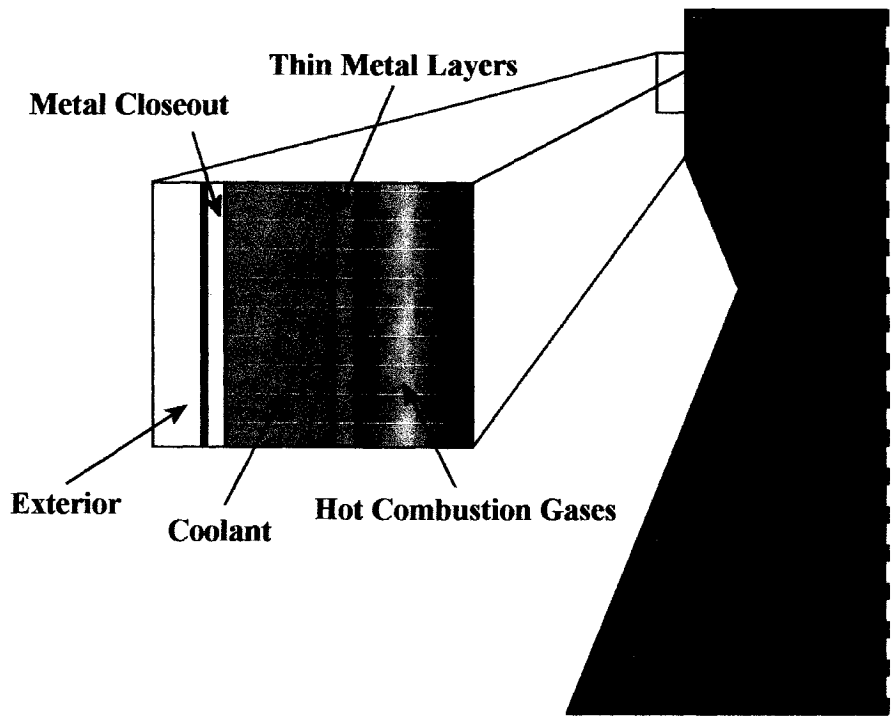

Figure 2.3. Regenerative Cooled Engine Wall Schematic

The hot combustion gases, convecting heat to the cooler thrust chamber wall, comprise the convective hot gas regime. The Bartz correlation, used to capture this interaction in the form of a convective heat transfer coefficient, is presented below in Eq. (2.8)[2]:

$$h_{g,r} = 0.026 \frac{k_{g,r}}{D_{hyd}} \left(\frac{C_{p_{g,r}}}{k_{g,r} \mu_{g,r}} \right)^{0.4} \left(\frac{\dot{m}_g D_{hyd}}{A_g} \right)^{0.8} \left(\frac{T_g}{T_{g,r}} \right)^{0.8} \phi_B \qquad \textbf{(2.8)}$$

Similarly, the convection on the coolant side between the heated thrust chamber wall and the cooler fuel coolant is again captured in the form of a convective heat transfer coefficient, given by the Colburn equation in Eq. (2.9)[2]:

$$h_{cool} = 0.023 \frac{k_{cool,f}}{D_{cool}} \left(\frac{C_{p_{cool,f}}}{k_{cool,f} \mu_{cool,f}} \right)^{0.4} \left(\frac{\dot{m}_{cool} D_{cool}}{A_{cool}} \right)^{0.8} \qquad \textbf{(2.9)}$$

Finally, the conduction through the chamber wall, characterized by linear 1-D heat transfer through a composite wall, is captured by calculating the thermal conductivity through the wall material layer or, in some cases, multiple material layers. The thermal conductivity of each of the layers is computed by interpolating in a look-up table that stores the thermal conductivity values as a function of temperature for each of the materials used in the wall. Once all three of these parameters are calculated, the thermal resistance through each of the regimes can then be calculated. A diagram showing the layout of the different resistance regimes is included below in Figure 2.4:

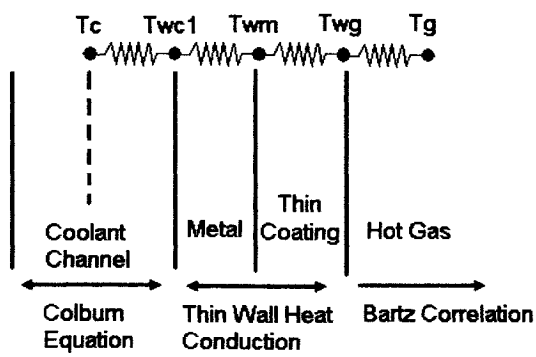

Figure 2.4. Simple Resistance Model (Note: Thin Coating is optional)

The equations used to calculate each of the three resistances for the hot side, coolant side and the chamber wall are given below in Eqs. (2.10), (2.11), and (2.12):

$$R_{hw} = \frac{1}{h_{g,r} A_{sm,hw}} \tag{2.10}$$

$$R_{cw} = \frac{1}{h_{cool} A_{sm,cw}} \tag{2.11}$$

$$R_{m} = \frac{t}{k_{m} A_{sm}} \tag{2.12}$$

With each of these resistances, the entire thermal interaction can be treated as a simple resistance model. This means that that the total heat transfer can be computed by obtaining the sum of the resistances and dividing the total temperature difference across the three regimes by this value, as outlined in Eq. (2.13):

$$\dot{Q} = \frac{T_g - T_{cool}}{R_{hw} + R_{cw} + R_m} \tag{2.13}$$

This heat transfer rate is a crucial parameter in the design and analysis of the engine, not only because it appears in the energy equation, but it also serves as an important industry metric for gauging the amount of cooling taking place.

In addition to the heat transfer rate, the two other important variables that must be computed in order to accurately characterize the heat transfer interaction are the hot wall side and cold wall side temperatures of the chamber. These can be solved for by using the previously derived heat transfer rate coefficients to generate a system of equations by equating all of the individual heat transfer rates through each of the three regimes. This corresponds to a steady state, one-dimensional energy balance across the chamber wall such that all of the heat transferred across the wall is absorbed by the coolant. In the

simplest case, where the wall itself is treated as a single layer, the heat transfer rate equations that are equated are shown below in Eqs.(2.14), (2.15) and (2.16)[2]:

$$\dot{Q}_{hw} = h_g A_{sm,hw}\left(H_{aw} - H_{hw}\right) \tag{2.14}$$

$$\dot{Q}_{cw} = h_c A_{sm,cw}\left(T_{cw} - T_{cool}\right) + q''_{fin} A_{fin} \tag{2.15}$$

$$\dot{Q}_m = \frac{k_m A_{sm}}{t}\left(T_{hw} - T_{cw}\right) \tag{2.16}$$

By setting these three equations equal to each other and rearranging variables, it is possible to solve for both the hot and cold wall temperatures. One important addition to take note of is the added heat flux term that is included in Eq. (2.15) - the cold-wall side equation. This term was added based on the approach used in Reference 21 to account for the additional heat transfer provided by the wetted surface area of the fins or lands that separate each coolant channel from its neighbor. A fin efficiency and heat flux term, which are calculated separately before being incorporated into Eq. (2.15), are shown below in Eqs. (2.17), (2.18) and (2.19)[2]:

$$m = \frac{2h_c\left(w_{fin} + dx\right)}{\left(k_m w_{fin} dx\right)} \tag{2.17}$$

$$\eta_{fin} = \frac{\tanh(m * hgt)}{m * hgt} \tag{2.18}$$

$$q''_{fin} = h_c\left(T_{cw} - T_{cool}\right)\eta_{fin} \tag{2.19}$$

Each equation is successively substituted into the next equation until the fin heat flux is determined and can be added to the cold wall side heat transfer rate equation. The hot and cold wall temperature equations derived from the heat transfer rate equations are given below in Eqs. (2.20) and (2.21):

$$T_{cw} = \frac{h_g A_{sm,hw}\left(H_{aw} - H_{hw}\right) - q''_{fin} A_{fin}}{h_c A_{sm,cw}} + T_{cool} \qquad \textbf{(2.20)}$$

$$T_{hw} = \frac{h_g A_{sm,hw} k_{m,i} A_{sm}}{t * t_{layer}}\left(H_{aw} - H_{hw}\right) + T_{cw} \qquad \textbf{(2.21)}$$

The equations for the hot and cold wall temperatures remain virtually the same regardless of the number of layers present in the chamber wall. However the T_{cw} term in Eq. (2.21) is replaced with an intermediate layer temperature.

2.6. Structural Analysis

Although not the primary focus of this study, the structural integrity of the coolant channels was still considered to a minor degree when running the design procedure. Based on studies performed in related research papers, the most significant potential modes of failure for coolant channels in the conditions presented here are primarily due to the bending stress in the channel wall and thermal stresses. The bending stresses are generated by the immense pressure in the combustion chamber and the thermal stresses are due to the temperature gradient across the channel wall between the hot combustion gases in the chamber and the cold fuel coolant in the channels. Low cycle fatigue and other structural failure mechanisms such as creep are typically not significant when compared to these other two failure mechanisms.[10][20] Since structural failure and stresses are not a primary concern in this study, they are simply calculated by the procedure and if they exceed the allowable stress limit a warning is displayed and the design should be adjusted as necessary. If this is the case, a more in depth structural or thermal stress analysis should be performed in order to obtain more accurate results and

verify that the stresses are indeed an issue. The equation used to calculate the bending stress in the coolant channel wall is given below followed by the equation for the longitudinal thermal stress[8][12][20]:

$$\sigma_{bending} = \frac{P_{cool} - P_g}{2}\left(\frac{w}{t}\right)^2 \tag{2.22}$$

$$\sigma_{thermal} = \alpha E(T_{hw} - T_{cw}) \tag{2.23}$$

Once calculated, the bending stress is compared to the yield stress of the chamber wall material to determine whether or not the current coolant channel design provided by the procedure is going to subject the engine to unacceptable stress levels. The maximum thermal stress is also displayed and can be compared to an appropriate critical stress if desired. It is important to note that these calculations are approximate and only accurate if the wall is comprised of a single material or, if multiple wall material layers are used, one of them is a dominant percentage of the wall composition compared to the other materials.

Another feature related to structural analysis that is embedded in the procedure addresses the issue of fabrication constraints. These geometric constraints are typically based on industry standards although they vary slightly from one company or production facility to the next based on the fabrication methods that are employed and the quality of the machinery. A table of fabrication criteria for the primary coolant channel geometric variables from three different sources was compiled by the authors of Reference 20 and is included below to show the approximate ranges for the parameters in question:

Table 2.1: Coolant Channel Fabrication Limits[20]
Fabrication Criteria Available in Literature

	Ref[23] (1998)	Ref[20] (1982)	Ref[21] (1976)
Channel width (w), in	≥0.02	≥0.03	≥0.04
Channel height (h), in	≤0.20	NA	NA
Land thickness (t), in	≥0.02	≥0.03	NA
Aspect ratio (h/w)	≤8	≤4	NA
Wall thickness (c), in	NA	≥0.025	≥0.028

The authors made the assumption that the values in the most recent paper from 1998 were probably the most relevant although it has been just over ten years now since that paper was published. These constraints can be embedded in the procedure's input file and prevent geometry from accidentally being entered that exceeds the current fabrication limits. This helps prevent wasted simulations that may generate results outside the realistic fabrication standards. As newer and more advanced fabrication methods are developed the constraints in the procedure can easily be modified to reflect the newest geometric data.

3. Results and Discussion

The results from the procedure developed for this thesis are presented in two different primary subsections: the first one describes the steps for verification procedures and cases used to ensure that the procedure actually produces accurate and reasonable results. The second section outlines a series of design trade studies that were performed in which several chambers and coolant channel profiles were designed using the Altair Lunar Lander main descent engine as a test platform.

3.1. Verification

As expected with developing any new procedure, it is critical that the generated results are verified against other pre-existing procedures or empirical data to ensure that the results are indeed correct. A systematic approach to the verification of this procedure was employed by verifying one aspect of the procedure at a time before successively activating another advanced module, such as friction or heat transfer. In addition, the complexity of the geometry and fluids used in the preliminary verifications was kept simple and employed ideal gases and water, before moving on to more advanced geometry and realistic fuel coolants like parahydrogen.

3.1.1. Inviscid Compressible Fluid

The first verification case that was run examined one of the most basic and fundamental fluid regimes: an ideal gas running through a converging-diverging duct with no heat addition or viscous effects. (A constant area duct was not employed since the case is trivial and results in constant fluid parameter trends). The fluid chosen for this

case was nitrogen, subjected to an inlet temperature and pressure that maintain the fluid as a superheated vapor. Several different methods were employed in order to run this case and verify levels of accuracy of different solution methodologies. These methods included an exact solution, an iterative analytical scheme and finally an iterative scheme that employs Refprop, forgoing the ideal analytical assumptions made in the previous two methodologies. The first method corresponding to the exact solution for quasi-one-dimensional flow, given below, was used as the foundation of the exact solution methodology, solving for P to provide an exact pressure distribution, while the additional equations listed subsequently were used to obtain the remaining fluid properties of interest (velocity, temperature, density and enthalpy)[17]:

$$\frac{\dot{m}}{A} = \frac{P_t}{\sqrt{T_t}} \sqrt{\frac{2g_c}{R} \frac{\gamma}{\gamma - 1} \left[\left(\frac{P}{P_t} \right)^{2/\gamma} - \left(\frac{P}{P_t} \right)^{(\gamma+1)/\gamma} \right]} \tag{3.1}$$

$$V = \sqrt{2C_p g_c T_t \left[1 - \left(\frac{P}{P_t} \right)^{(\gamma+1)/\gamma} \right]} \tag{3.2}$$

$$T = T_t - \frac{V^2}{2C_p g_c} \tag{3.3}$$

$$\rho = \frac{\dot{m}}{AV} \tag{3.4}$$

$$H = C_p T \tag{3.5}$$

The iterative schemes both employed the previously discussed governing equations. The table shown below summarizes the inlet parameters used in this first verification case followed by a plot showing the area distribution used for the coolant channels as a function of axial position, where 0 represents the chamber throat:

Table 3.1. Frictionless Compressible Fluid Parameters

Procedure Parameters	Value	Units
Number of Coolant Channels	180	n/a
Total Coolant Mass Flowrate	2.95	lbm/s
Inlet Static Temperature	540	Rankine
Inlet Static Pressure	49.5	psi
Inlet Total Temperature	540.54	Rankine
Inlet Total Pressure	49.67	psi
Specific Heat Ratio	1.4	n/a
Ideal Gas Constant	55.15	(ft*lbf)/(lbm*R)
Specifc Heat (constant pressure)	0.248	Btu/(lbm*R)

Note: Not all of these inlet parameters are required by each of the three different solution methods

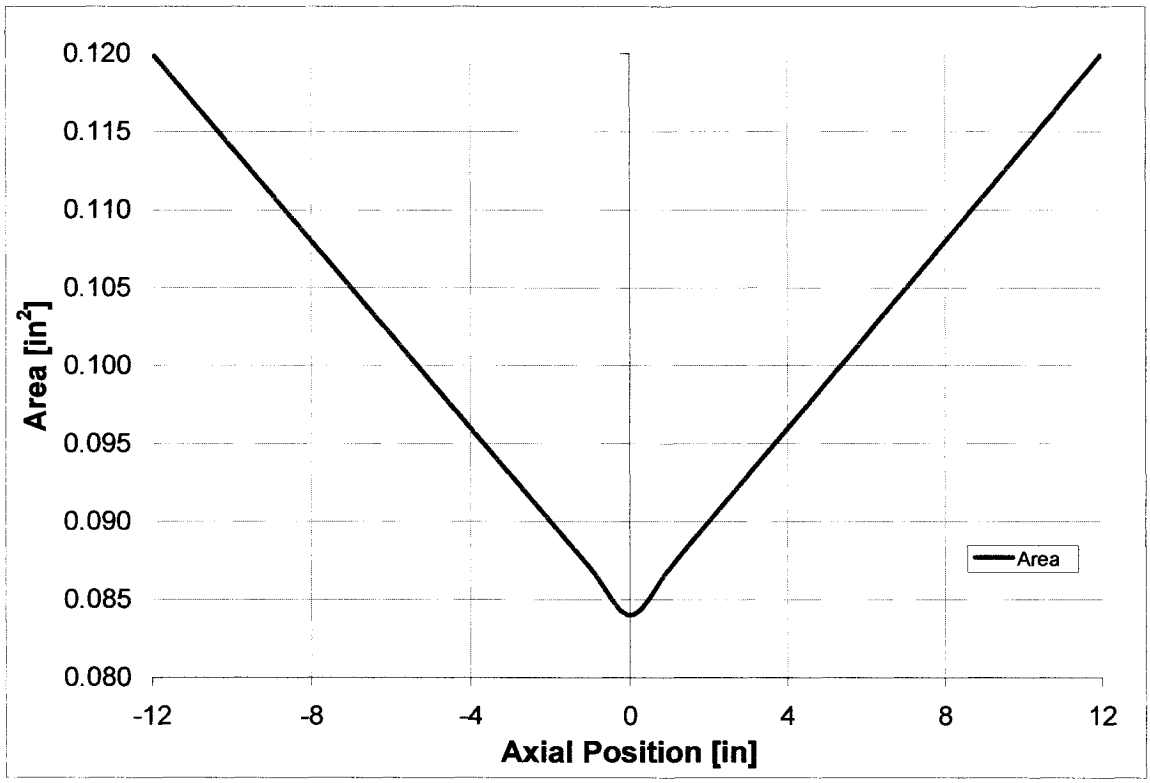

Figure 3.1. Inviscid Compressible Fluid Area Distribution

It is important to note in this plot, and in all future plots, that negative axial position designates a location upstream of the chamber throat and vice versa. Because the coolant flow enters the channels downstream of the throat and travels up to the injector, the fluid trends depicted in each figure begin on the right side of the plot and propagate to the left. The results from all three of these methods are shown below in the following plots which

display the trends of several of the primary variables as they change along the length of the coolant channel:

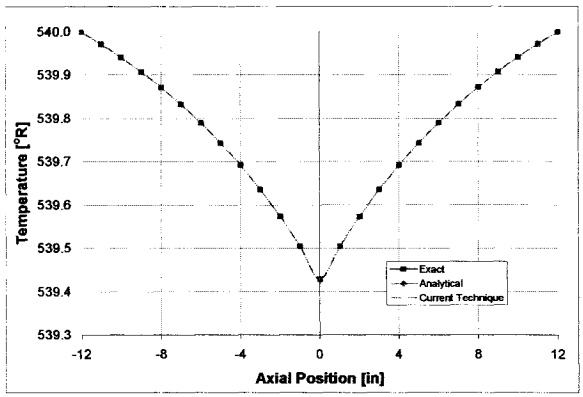

Figure 3.2. Inviscid Compressible Fluid Temperature Distribution

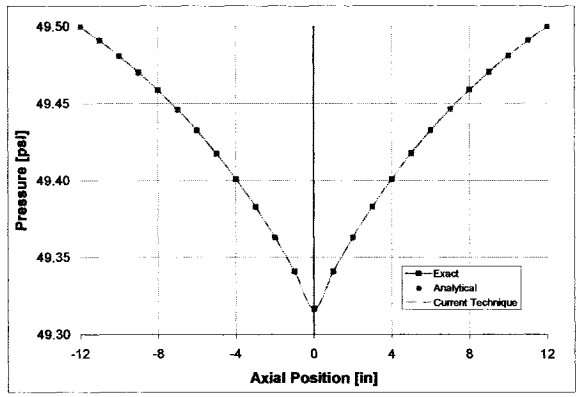

Figure 3.3. Inviscid Compressible Fluid Pressure Distribution

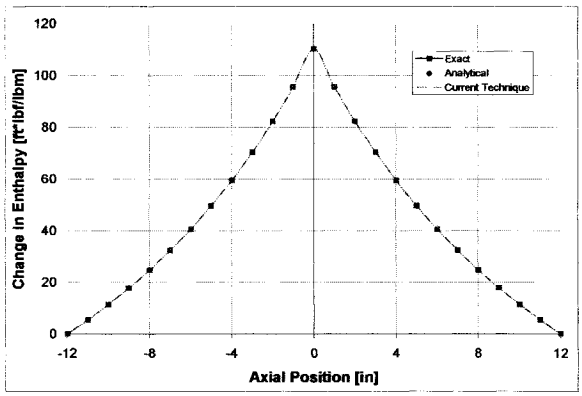

Figure 3.4. Inviscid Compressible Fluid Change in Enthalpy (H_{inlet}-H_i) Distribution

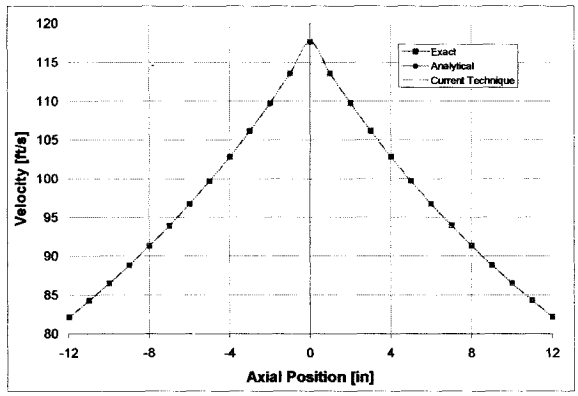

Figure 3.5. Inviscid Compressible Fluid Velocity Distribution

Note: These figures and all future plots of fluid properties must be read from right to left since the coolant flow path begins at the downstream chamber exit and proceeds upstream, in the opposite direction of the chamber flow, towards the injector.

It should be clear from these four plots that the procedures developed in Matlab, using either analytical equations that make ideal gas assumptions, or treat the substance as a real fluid by making calls to Refprop, closely agree with the exact solution. It should be noted here that only 24 control volumes were used in this analysis, which is a fairly course grid. Given that the three methods already provide virtually identical results a

finer grid with more control volumes was not employed. However, future studies with more complex geometry and fluid regimes may require a finer grid which will be taken into consideration and addressed later. With this verification successfully completed, it was then deemed necessary to verify the procedure using an incompressible fluid.

3.1.2. Inviscid Incompressible Fluid

The next test case that was run used water as the coolant fluid to verify that the procedure can correctly handle incompressible fluids. A constant area and a converging-diverging area distribution for the coolant channels were employed and a summary of the inlet parameters is given below in Table 3.2:

Table 3.2. Inviscid Incompressible Fluid Parameters

Procedure Parameters	Value	Units
Number of Coolant Channels	180	n/a
Coolant Inlet Static Temperature	539.99	Rankine
Coolant Inlet Static Pressure	49.00	psi
Total Coolant Mass Flowrate	85.42	lbm/s
Coolant Channel Widths	0.30	in

In order to verify that the results from the water test case were correct, another existing fluids procedure called Linesolve[4][5], was employed to run the same test cases. Linesolve is a quasi one-dimensional procedure that directly solves the governing fluids equation in elliptic differential form versus the parabolic control volume marching scheme used in the current procedure. The results from this verification case are included below for the converging-diverging area case (the constant area case is trivial, the results being all straight lines, and agreement is essentially perfect):

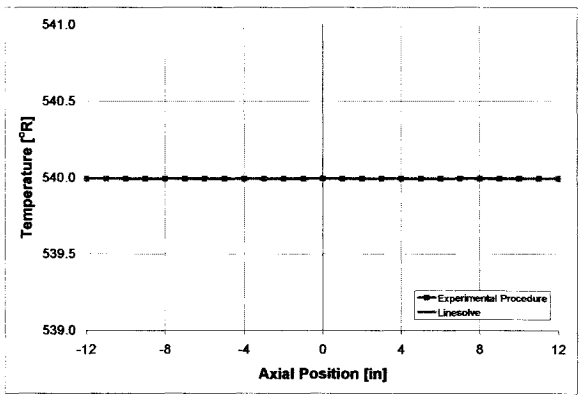

Figure 3.6. Inviscid Incompressible Fluid Temperature Distribution (variable area)

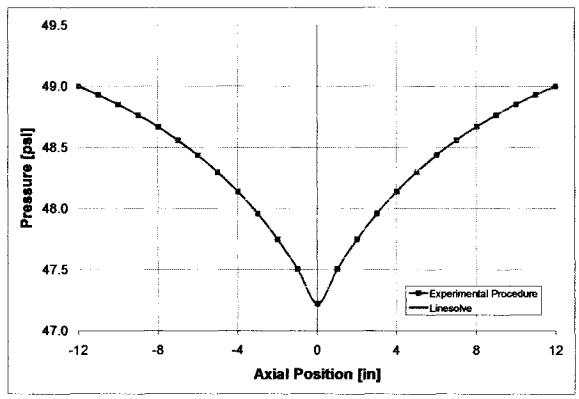

Figure 3.7. Inviscid Incompressible Fluid Pressure Distribution (variable area)

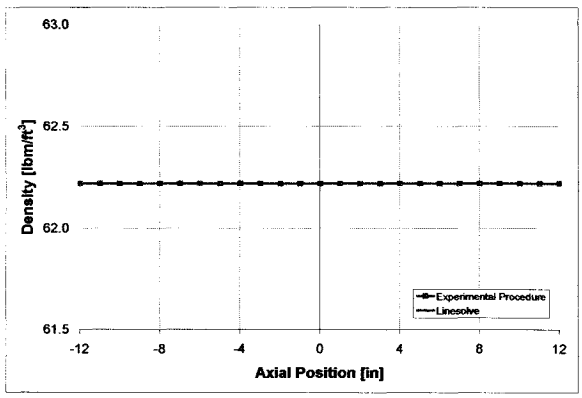

Figure 3.8. Inviscid Incompressible Fluid Density Distribution (variable area)

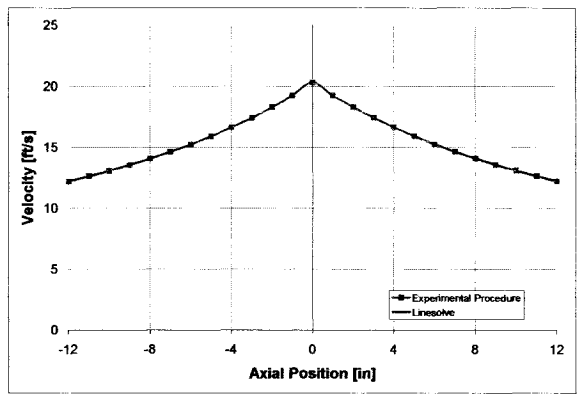

Figure 3.9. Inviscid Incompressible Fluid Velocity Distribution (variable area)

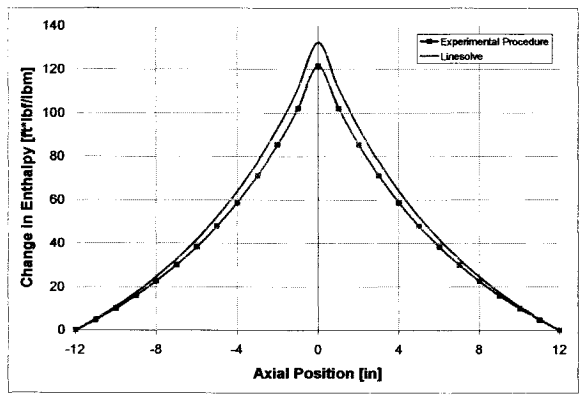

Figure 3.10. Inviscid Incompressible Fluid Change in Enthalpy (H_{inlet}-H_i) Distribution (variable area)

With consistent agreement in all of the plots shown, it is safe to proceed to more advanced cases that take into account friction, more realistic fluids and channel area distributions, and ultimately heat transfer to the coolant.

3.1.3. Viscous Compressible Fluid

Subsequently, a verification case was run using nitrogen but this time incorporated friction into the simulation. Two different coolant channel area distributions were employed: a constant area distribution of 0.09 in^2 and the variable converging-diverging distribution used in a previous verification (Figure 3.1) with similar inputs to that of the first verification case as well. As in the inviscid incompressible fluid case, Linesolve was again used to verify that the results were valid. The table below lists all of the parameters used in this verification case:

Table 3.3. Viscous Compressible Fluid Parameters

Procedure Parameters	Value	Units
Number of Coolant Channels	180	n/a
Coolant Inlet Static Temperature	539.30	Rankine
Coolant Inlet Static Pressure	47.77	psi
Total Coolant Mass Flowrate	2.50	lbm/s
Coolant Channel Widths	0.30	in
Coolant Channel Roughness	1.9E-05	n/a

The following two sets of plots depict how the various important fluid variables change as a function of axial position within the coolant channel using both Linesolve and the current procedure developed thus far. It is important to note once again that the coolant channel inlet is downstream of the throat and thus lies on right side of each plot while the coolant channel exit at the main injector is on the left side of each plot, upstream of the throat:

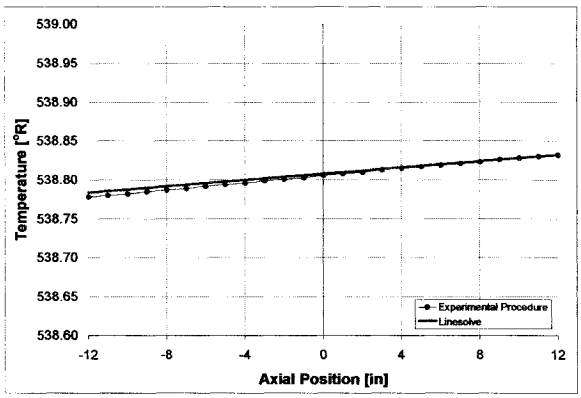

Figure 3.11. Viscous Compressible Fluid Temperature Distribution (constant area)

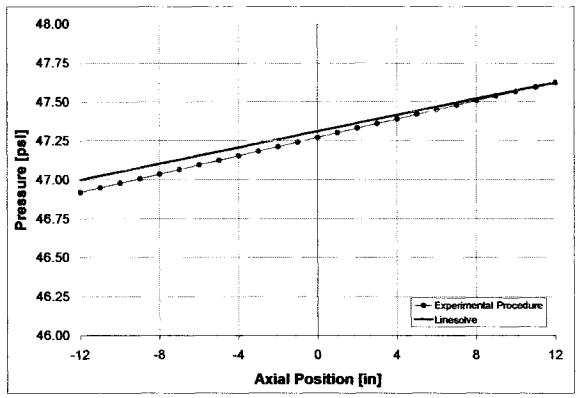

Figure 3.12. Viscous Compressible Fluid Pressure Distribution (constant area)

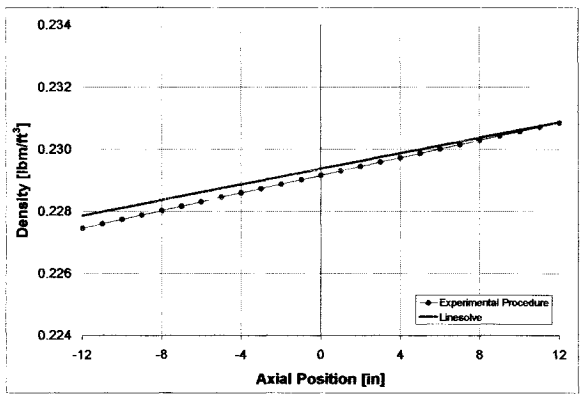

Figure 3.13. Viscous Compressible Fluid Density Distribution (constant area)

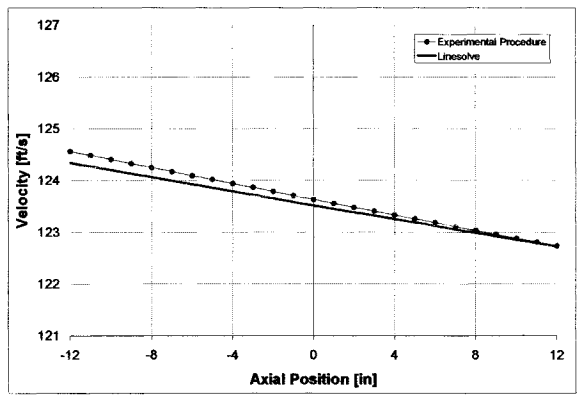

Figure 3.14. Viscous Compressible Fluid Velocity Distribution (constant area)

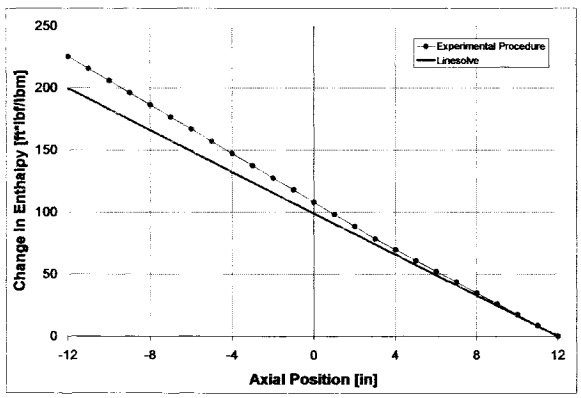

Figure 3.15. Viscous Compressible Fluid in Enthalpy (H_{inlet}-H_i) Distribution (constant area)

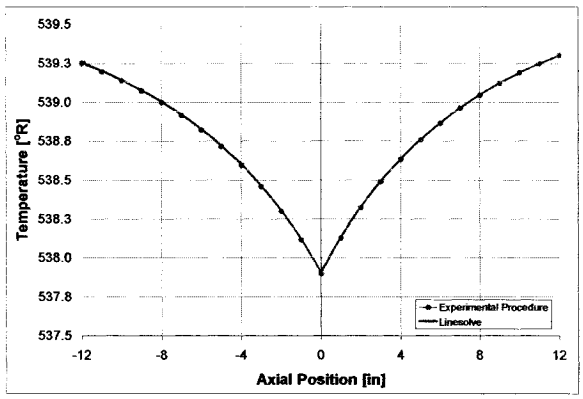

Figure 3.16. Viscous Compressible Fluid Temperature Distribution (variable area)

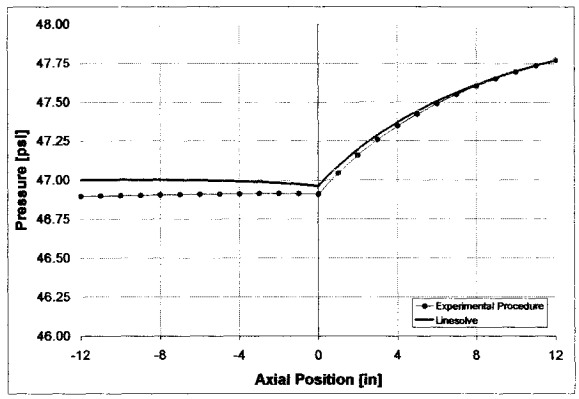

Figure 3.17. Viscous Compressible Fluid Pressure Distribution (variable area)

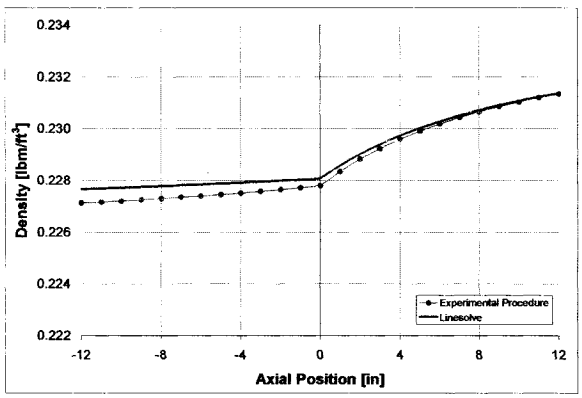

Figure 3.18. Viscous Compressible Fluid Density Distribution (variable area)

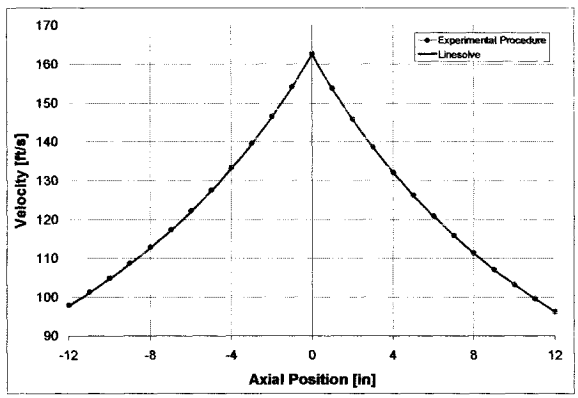

Figure 3.19. Viscous Compressible Fluid Velocity Distribution (variable area)

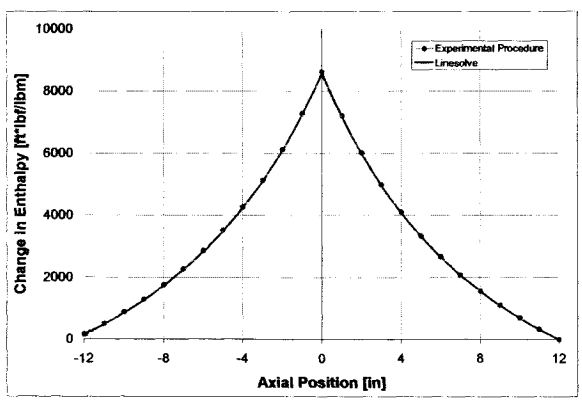

Figure 3.20. Viscous Compressible Fluid Change in Enthalpy (H_{inlet}-H_i) Distribution (variable area)

From these figures it is quite clear that the new experimental procedure closely mimics the results provided by Linesolve for all five of the primary fluid variables. The slight discrepancies between the lines are all of small orders of magnitude and can be attributed to the considerably different manner in which each of the procedures solves for the fluid variables. For all of these steady flow simulations it is important to note that the current procedure reduces solution times drastically compared to Linesolve, converging in a few seconds versus several hours. Given that there is relatively close agreement between Linesolve and the experimental procedure, it is reasonable to proceed with the assumption that the new procedure is accurately capturing the behavior of the fluid in the coolant channels.

3.1.4. Viscous Incompressible Fluid

To complete the primary verification of the procedure, water was again used to verify that an incompressible fluid can be accurately handled by the procedure, this time incorporating friction. Once again, the same constant area distribution and a converging-diverging area distribution similar to the one used in the viscous compressible verification, were used for the coolant channels. The table below lists the parameters used in the verification case followed by a small sampling of plots comparing the procedure results with Linesolve for both the constant and variable area cases:

Table 3.4. Viscous Incompressible Fluid Parameters

Procedure Parameters	Constant Area	Variable Area	Units
Number of Coolant Channels	180	180	n/a
Coolant Inlet Static Temperature	539.99	539.99	Rankine
Coolant Inlet Static Pressure	49.67	49.89	psi
Total Coolant Mass Flowrate	48.94	28.85	lbm/s
Coolant Channel Widths	0.30	0.30	in
Coolant Channel Roughness	1.90E-05	1.90E-05	n/a

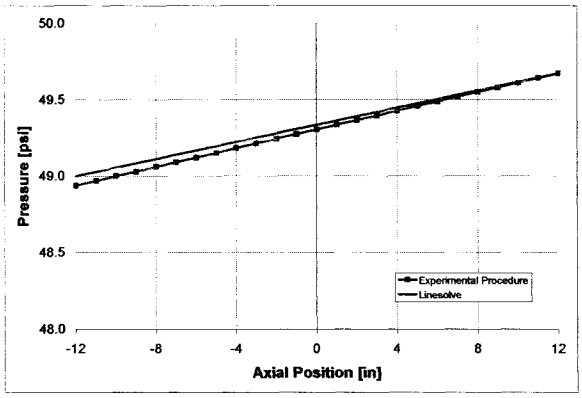

Figure 3.21 Viscous Incompressible Fluid Pressure Distribution (constant area)

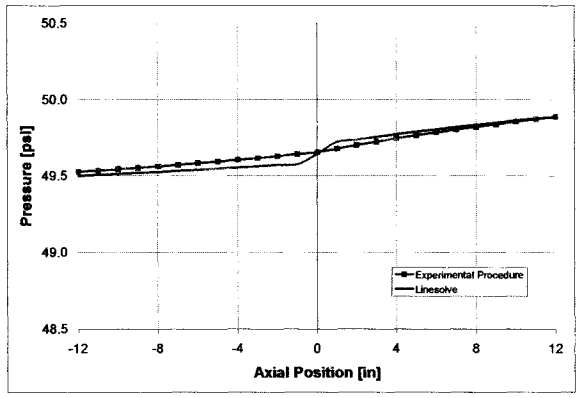

Figure 3.22 Viscous Incompressible Fluid Pressure Distribution (variable area)

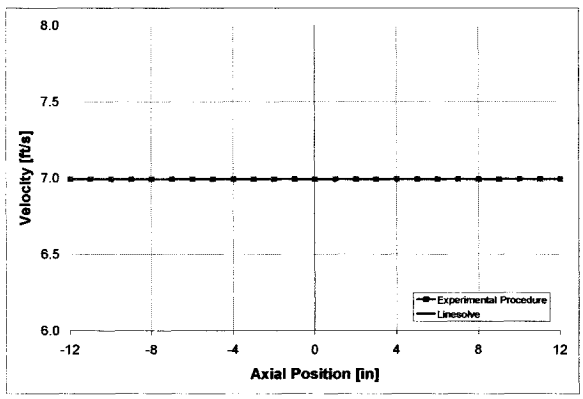

Figure 3.23 Viscous Incompressible Fluid Velocity Distribution (constant area)

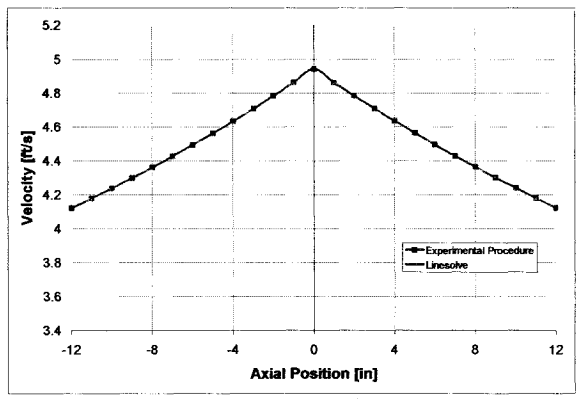

Figure 3.24 Viscous Incompressible Fluid Velocity Distribution (variable area)

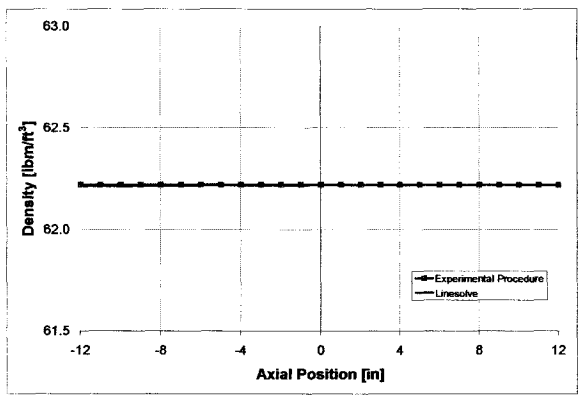

Figure 3.25. Viscous Incompressible Fluid Density Distribution (constant & variable area)

Again it is clear that the current procedure can handle an incompressible fluid in inviscid and viscous cases and closely matches Linesolve's results. The plots for both these cases

are rather benign primarily due to the limited changes an incompressible fluid such as water can go through in the coolant channels at the mass flow rates and pressures chosen. Now that the procedure has been verified for both compressible and incompressible fluids in friction and frictionless environments using constant and variable area channels, the next set of verifications must examine the fluid behavior when heat transfer from the combustion chamber is added.

3.1.5. Simple Heat Transfer

Before running a test case to verify the entire heat transfer module, which provides the main fluid module with accurate values for the heat transfer rate, $\dot{Q}$, used in the energy equation, it was important to verify the accuracy of this energy balance. Up to this point, all verification cases that were run had the $\dot{Q}$ term in the energy equation set to zero, eliminating the effects of heat transfer to allow for simpler verification methods. In order to ensure that the energy equation is correct, a constant heat transfer rate was chosen and applied along the length of the coolant channel into each control volume. This value was not calculated using the heat transfer correlations discussed previously in the heat transfer module but was simply chosen as a hypothetical realistic heat transfer rate input. Two studies were performed: one using parahydrogen and one using methane, two fluids that will be the primary candidates for fuel coolants in future test cases. In order to validate the results generated by each of these studies, the temperature distributions resulting from the constant heat transfer rate input were compared with an analytical equation from Reference 14 that predicts the mean temperature profile for internal flow in a pipe:

$$T_{mean}(x) = T_{mean,i} + \frac{q'' A_p}{\dot{m} C_p} x \qquad (3.6)$$

This equation however assumes that the channels are circular tubes and that the heat is entering from all sides of the tube, which is why the wetted perimeter term, A_p, appears in the equation. Thus, in order to modify the equation to work with the rectangular channels and heat transfer from only the single chamber side, this term was replaced with the coolant channel's width. The following tables lists the values of the parameters used in this equation and the inlet parameters and geometry used in the procedure test cases:

Table 3.5. Parameters for use with the Analytical Temperature Equation

Analytical Parameters	Parahydrogen	Methane	Units
$T_{mean,i}$	57.94	210	Rankine
q"	6.43	6.43	BTU/(in^2*s)
Coolant Channel Width	0.1	0.1	inches
Coolant Mass Flowrate	0.034	0.084	lbm/s
Cp	3.793	0.925	BTU/(lbm*R)
x (position in channel)	0<x<24	0<x<24	inches

Table 3.6. Parameters for use with the Experimental Procedure

Procedure Parameters	Parahydrogen	Methane	Units
Coolant Inlet Static Temperature	57.94	210	Rankine
Coolant Inlet Static Pressure	1018.3	2299	psi
Coolant Mass Flowrate	0.034	0.084	lbm/s
Coolant Channel Area	0.03	0.03	in^2
Chamber Hydraulic Diameter	12	12	in
Heat Transfer Rate (Qdot)	0.643	0.643	BTU/s
Heat Flux (q")	6.43	6.43	BTU/(in^2*s)

The two figures below show how the analytical results predicted using Equation (3.6) correlate with the coolant temperature profile calculated using the current procedure:

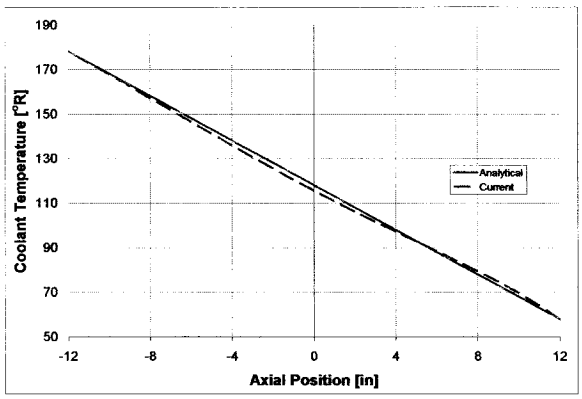

Figure 3.26. Parahydrogen Heat Transfer Rate Temperature Comparison

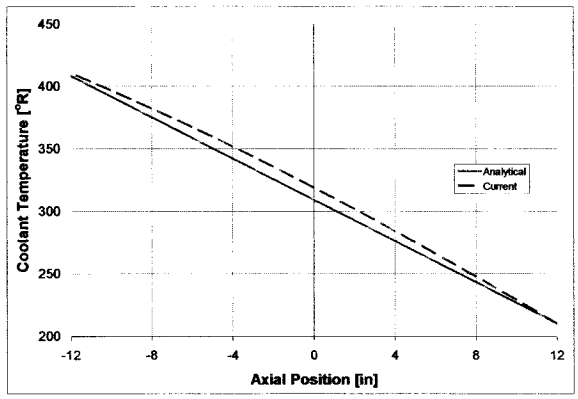

Figure 3.27. Methane Heat Transfer Rate Temperature Comparison

These two plots clearly indicate that the energy balance in the current procedure is indeed handling the addition of heat correctly. The difference between the analytical and current predicted results stem primarily from the fact that the analytical equation assumes that Cp is constant, whereas the current procedure uses a variable distribution incorporating real fluid properties into all of the calculations. With this simple verification complete, it is now reasonable to move on to verify the heat transfer module and ensure that it can produce accurate values for the heat transfer rate and heat flux, as well as the hot wall and cold wall side temperatures.

3.1.6. RL10 Comparison

One engine study that is very prominent and is often used as a reference for technical verification is the RL10A-3-3A Rocket Engine Modeling Project published in 1997 as a NASA Technical Memorandum[2]. It contains extensive information on how the engine was modeled, the procedures and correlations used and a large quantity of experimental data. It is also one of the few reports that contain plots of fluid properties and heat transfer related variables in the regenerative coolant channels, as a function of

axial position with respect to the thrust chamber. This makes it a promising candidate for results verification although the engine itself has many complexities (both geometric and fluidic) and uses the older tubular-wall cooling jacket instead of the more widely used coolant channels. This of course led to some technical issues which have been encountered by other researchers performing related coolant channel studies who comment that "Validating the results with the RL10-3-3A presented a slight discomfort due to the significant difference in the geometry." And that, "[b]ecause the RL10 employs a tubular walled geometry where we have chosen to consider a rectangular coolant channel wall for the regenerative cooling passages, we believed the correction factors could be erroneous."[20] An additional complication arises from the fact that the RL10's coolant channel is a one-and-a-half pass design, rather than a single pass, which means that the tubes double back on themselves in the lower portion of the chamber (see Figure 3.28):

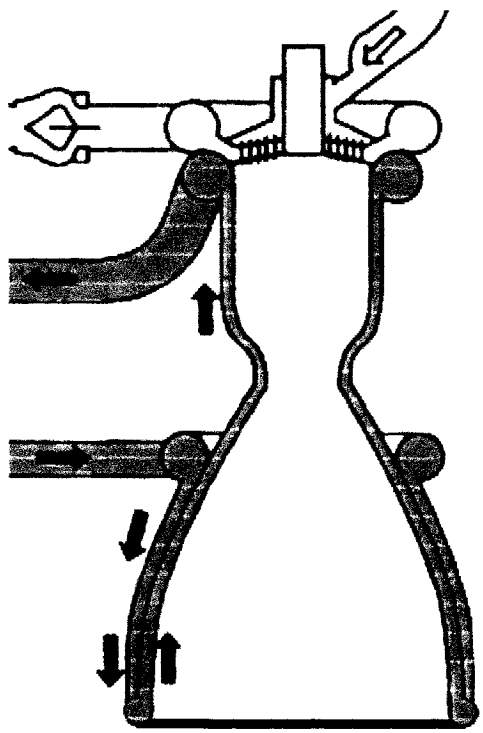

Figure 3.28. RL10 schematic illustrating 1½ pass design[2]

Regardless, comparing results with the published RL10 data still provides a valuable level of verification. It must be understood however that generating a very accurate match is nearly impossible, especially since many different correction factors were used in the original study to help correlate their results with actual engine test data.

The primary reason for comparing results with the RL10 is to provide verification of the heat transfer module within the current procedure, especially because the main equations used in calculating the various heat transfer coefficients were taken directly from the RL10-3-3A report. All of the input parameters and geometry required to run this case were taken directly from this study and associated files, although the coolant channel height profile had to be smoothed slightly. For instance there is a large discontinuity part way up the chamber due to the one-and-a-half pass design which results in erroneous data spikes. The following set of plots show the results from the current procedure versus all of the various runs that were shown and discussed in the RL10-3-3A report:

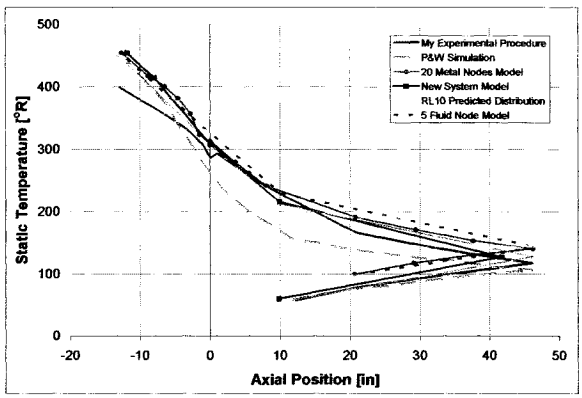

Figure 3.29. RL10 Coolant Static Temperature Comparisons

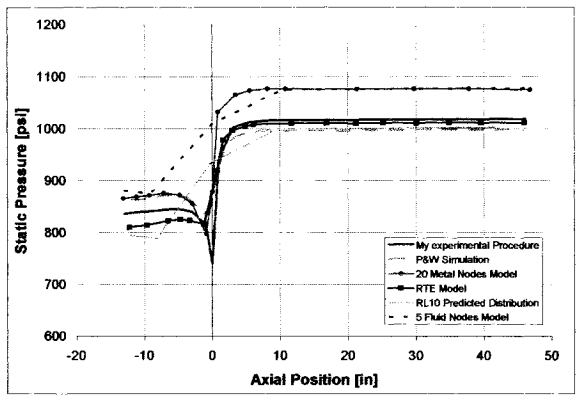

Figure 3.30. RL10 Coolant Static Pressure Comparisons

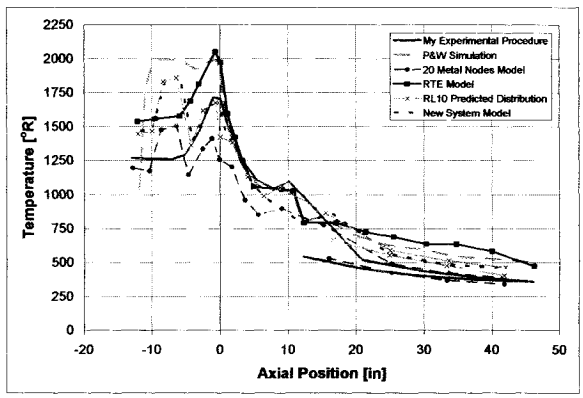

Figure 3.31. RL10 Hot Wall Temperature Comparisons

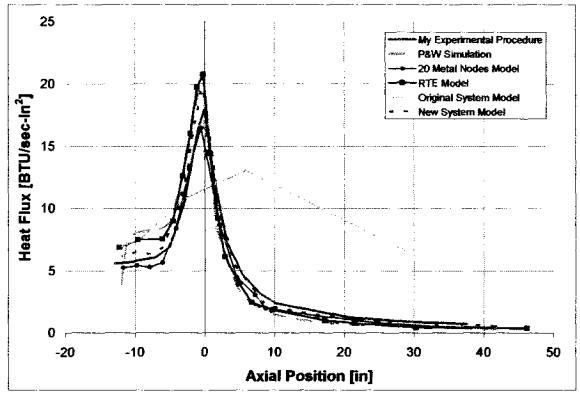

Figure 3.32. RL10 Heat Flux Comparisons

Examining these plots, it is obvious that there is a wide range of results produced by each of these various tests that makes it difficult to obtain a truly exact match. However, in all of the cases, the results produced by the current procedure closely follow the trends in the other models and distributions. Examinations of Figure 3.29 - Figure 3.32 shows that all of the tests were apparently not run on the entire coolant channel since many of the data series do not include the initial overlapping portion of the coolant tubes.

With the completion of this comparison, it was deemed that the similarity between all of the trends tabulated in the RL10-3-3A and the current procedure verifies

that the procedure is working correctly and is accurate enough to adapt to cases for which it was not explicitly designed.

3.1.7. Effect of Grid Density

As briefly mentioned previously, an important factor that plays a critical role in solution accuracy, as well as procedure runtime, is computational grid density. In this procedure, grid density is defined by the number of control volumes into which the coolant channel is divided. For most of the basic cases a small number of control volumes, typically twenty-four, is used in order to keep the procedure runtime on the order of a few minutes. However, it is important to verify that this number of control volumes accurately captures the behavior of the fluid in the coolant channels. Several test cases were run with the number of control volumes being increased each time from four, to twenty-four, and finally to fifty, using the same fluid input parameters and chamber geometry in all three cases. The table shown below lists the inlet parameters, taken primarily from the RL-10 test case, followed by a plot of the chamber inner radius contour that was used:

Table 3.7. Parameters used for Analysis Grid Density Verification

Procedure Parameters	Value	Units
Chamber Static Temperature	5888	Rankine
Chamber Static Pressure	475	psi
Chamber Mixture Ratio	5.0	n/a
Chamber Wall Thickness	0.013	inches
Chamber Mass Flowrate	37.36	lbm/s
Number of Coolant Channels	180	n/a
Coolant Inlet Static Temperature	57.94	Rankine
Coolant Inlet Static Pressure	1018.3	psi
Coolant Mass Flowrate	0.0338	lbm/s
Coolant Channel Area	0.03	in^2

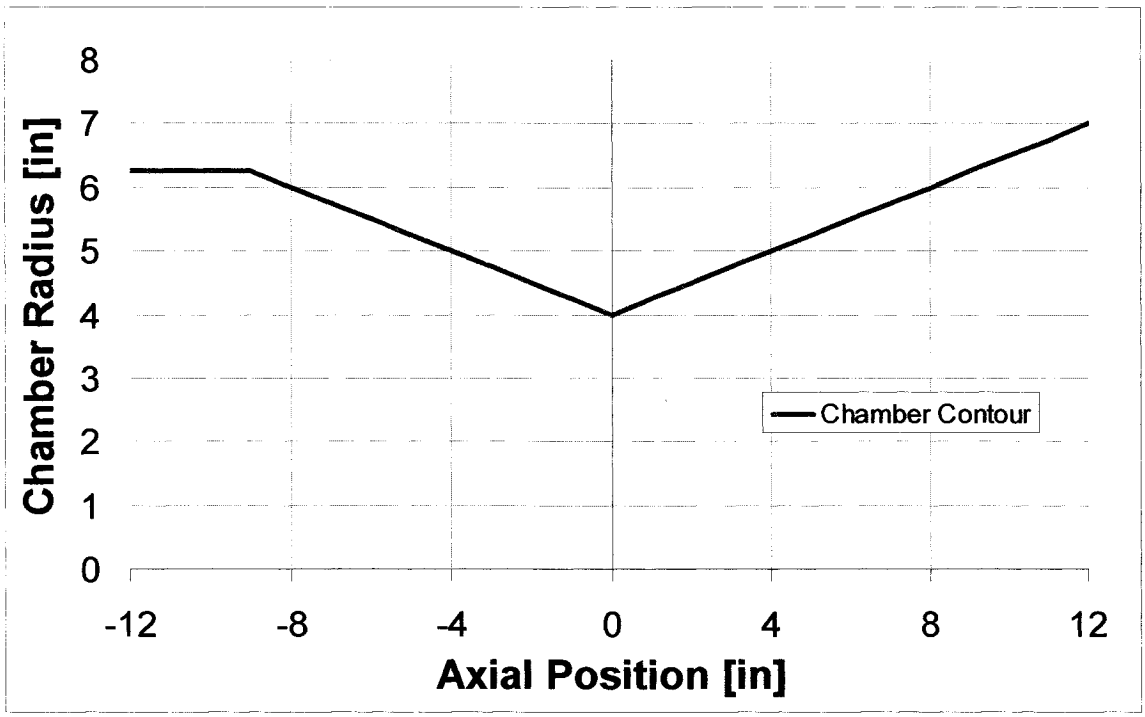

Figure 3.33. Combustion Chamber Contour for Analysis Grid Density Verification

The test cases were all run in analysis mode using parahydrogen as the coolant with a stainless steel chamber wall. A predetermined constant coolant channel contour was used, resulting in a uniform area distribution, and in order to give this verification the most realistic settings possible, both friction and heat transfer were enabled. The following set of three plots illustrate the effect of grid density on the predicted coolant pressure, temperature and velocity along the length of the coolant channels:

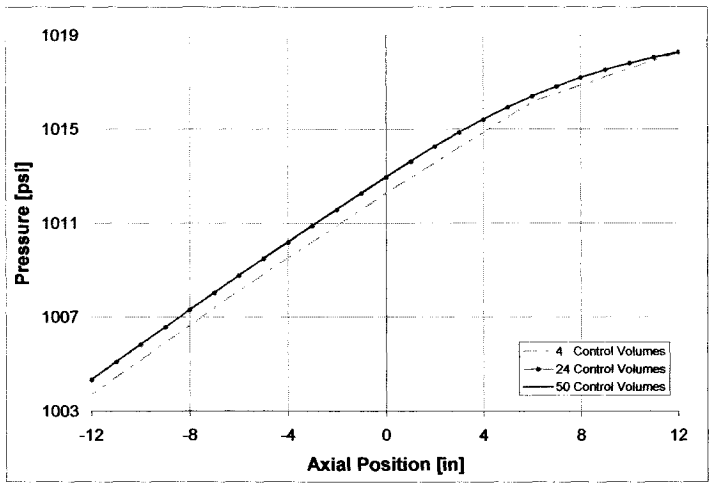

Figure 3.34. Analysis Grid Density Verification Pressure Distribution

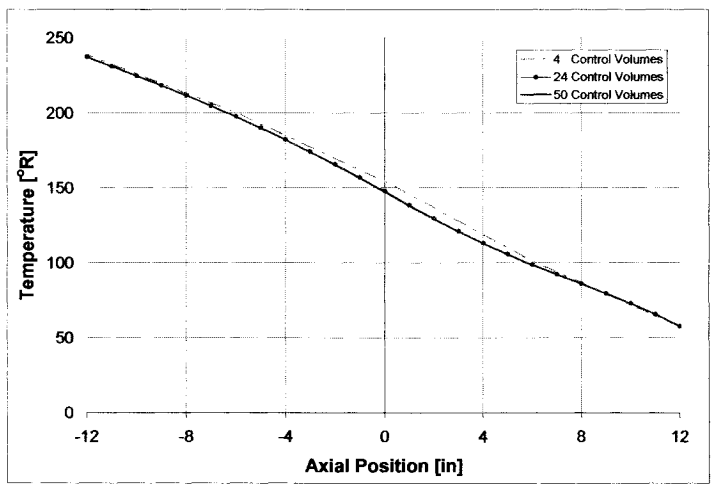

Figure 3.35. Analysis Grid Density Verification Temperature Distribution

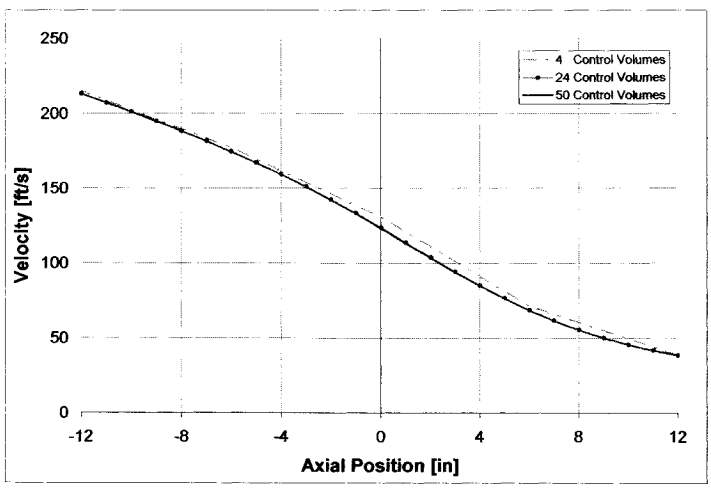

Figure 3.36. Analysis Grid Density Verification Velocity Distribution

It is quite evident from these three figures that there definitely is a perceptible difference between the results using only four control volumes versus twenty-four control volumes. However, there is no obvious difference between the results using twenty-four control volumes and fifty control volumes. Thus, it is safe to assume that the chosen baseline value of twenty-four control volumes accurately captures the behavior of the coolant fluid. This test case however was run using a constant coolant channel area distribution as mentioned previously and thus does not put the fluid through any extreme changes that might result in more complex fluid property distributions.

In order to verify that twenty-four control volumes is still sufficient to accurately capture all of the fluctuations the fluid would undergo in a variable area channel, a design case was run that allowed the procedure to modulate the coolant channel heights in order to achieve a prescribed hot-wall temperature. The same chamber contour from the previous grid density verification case (Figure 3.33) was again used and the table below summarizes the input parameters:

Table 3.8 Parameters used for Design Grid Density Verification

Procedure Parameters	Value	Units
Chamber Static Temperature	5888	Rankine
Chamber Static Pressure	475	psi
Chamber Mixture Ratio	5.0	n/a
Chamber Wall Thickness	0.013	inches
Chamber Mass Flowrate	37.36	lbm/s
Number of Coolant Channels	180	n/a
Coolant Inlet Static Temperature	57.94	Rankine
Coolant Inlet Static Pressure	1018.3	psi
Coolant Mass Flowrate	0.0338	lbm/s
Coolant Channel Width	0.1	in
Coolant Channel Inlet Height	0.3	in
Prescribed Hot-wall Temperature	1200	Rankine

As before, a series of three plots included below show how the pressure, temperature and velocity are affected by grid density. An additional plot depicts the area distribution that was generated by the procedure to maintain a constant hot-wall temperature of 1200 ^{o}R:

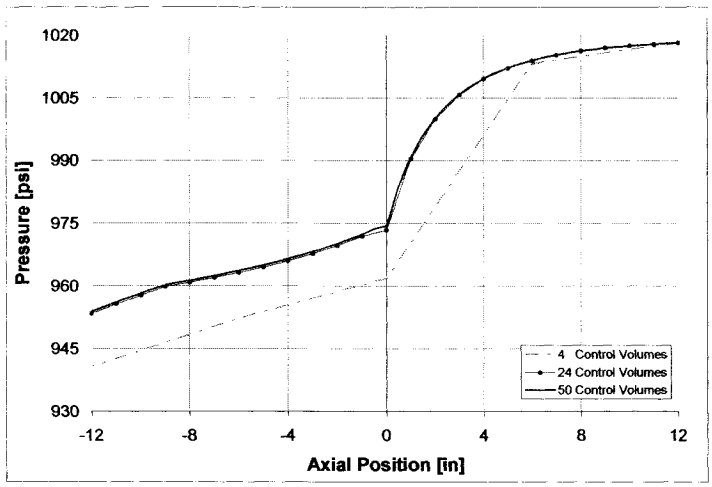

Figure 3.37. Design Grid Density Verification Pressure Distribution

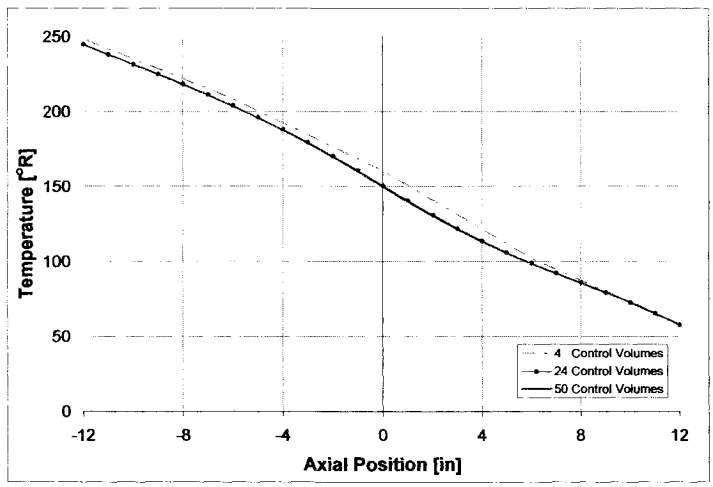

Figure 3.38. Design Grid Density Verification Temperature Distribution

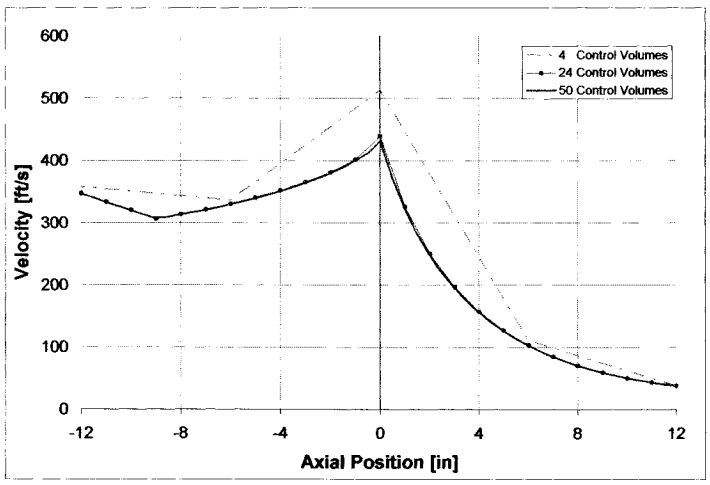

Figure 3.39. Design Grid Density Verification Velocity Distribution

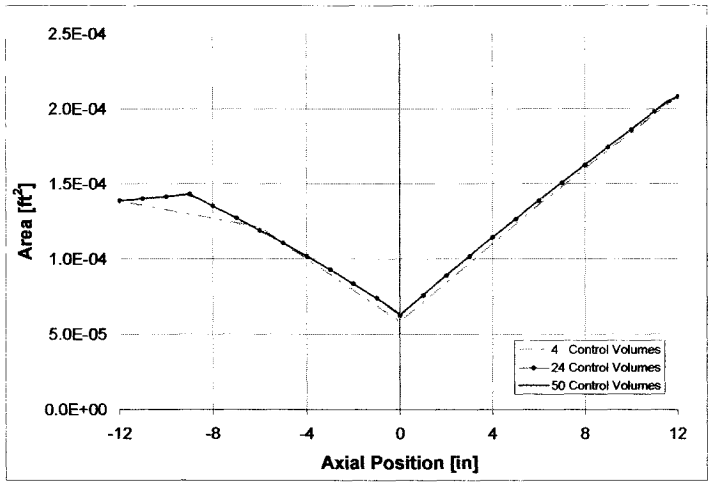

Figure 3.40. Design Grid Density Verification Area Distribution

Again, we see that the case where only four control volumes were used is too coarse and clearly does not accurately capture all of the fluctuations in the fluid variables. However, the twenty-four control volume case still appears to match the fifty control volume case very well with only slight deviations at the more severe inflection points. Given this data, it can be concluded that twenty-four control volumes is a sufficient baseline grid density and is capable of producing accurate results. One should also notice the area distribution (Figure 3.40) generated by the procedure in this design case is clearly variable and, as expected, its overall contour closely matches the shape of the chamber contour since smaller channel areas are needed at the throat to increase cooling and vice versa.

3.1.8. Typical Procedure Solution Times

All of the verification cases and trade studies using this procedure were run on a Dell XPS system with an Intel Pentium Dual Core 2.80GHz processor utilizing 2.00 GB of RAM. The computer is running Windows XP with Service Pack 3 and MATLAB

version 7. For analysis cases using fifty control volumes or less, running viscous or inviscid flow and using either a constant or converging-diverging coolant channel area distribution, solution times are typically under five seconds. When heat transfer is included as well, solution times for twenty-four control volumes or less are typically under one minute while running fifty control volumes increases the runtime to just over a minute. Given that rapid solution times with reasonable accuracy was a primary goal and motivation for the development of this procedure, these times are very satisfactory and encouraging.

When the procedure is executed in design mode, solution times are longer because the area distribution must be constantly modified forcing the procedure to iterate on each control volume a significantly greater number of times. However, the solution times were still very acceptable. In every case that was run, solution times were always under five minutes and in many cases results were achieved in less than four minutes. This allows numerous design cases to be run in a short period of time which is critical for a procedure like this that has been developed for trade studies and rapid result comparisons. Further optimization of the design routine could still be performed by employing a more efficient and complex algorithm, which would result in even shorter solution times. The current algorithm is a simple yet efficient "divide and conquer" routine but it may be possible to utilize error calculations to further narrow each of the successively smaller search domains. Unfortunately this level of optimization lies outside the scope of this study.

3.2 Design Trade Studies

With verification completed, the primary objective of performing a coolant channel profile preliminary design for a particular engine can finally be addressed. The chosen application for this set of trade studies is the main descent engine that is currently being designed and considered for NASA's Altair Lunar Lander. The proposed engine is a LOX/LH_2 expander cycle liquid engine operating in a moderate thrust range, very similar to and actually a direct descendent of the previously discussed RL10 engine.

3.2.1 Design Case Setup

The primary two design specifications that need to be met are a thrust of approximately 9000 lbf and a vacuum I_{sp} of about 448 seconds. Using the specific impulse as a design point, a publically available one-dimensional equilibrium combustion code called Cpropep[11] was used to obtain characteristic velocities, nozzle area ratios and chamber temperatures for a range of chamber pressures and mixture ratios. Several theoretical rocket engine chambers with conical nozzles were then designed using these parameters and following the methods outlined in Chapter 3 of Reference 22 and Chapter IV of Reference 12. Once the chamber geometry was defined, all of the requisite input conditions were specified using Cpropep data along with data from the RL-10 engine due to their similarities. The table below summarizes all of the input conditions that are common between the different chambers:

Table 3.9. Design Trade Study Common Input Parameters

Procedure Parameters	Value	Units
Number of Coolant Channels	180	N/A
Coolant Inlet Static Temperature	57.94	Rankine
Coolant Channel Roughness	1.90E-05	n/a
Chamber Wall Thickness	0.013	inches
Chamber Mass Flowrate	20.089	lbm/s
Coolant Channel Land Width	0.03	inches

As mixture ratio and chamber pressure are varied, the geometry of the chamber also varies slightly as well. Thus, for each of the chosen chamber pressures and mixture ratios, a unique chamber is produced. Included in the figures below are the geometric profiles of each of the chambers generated for this study (nine in total):

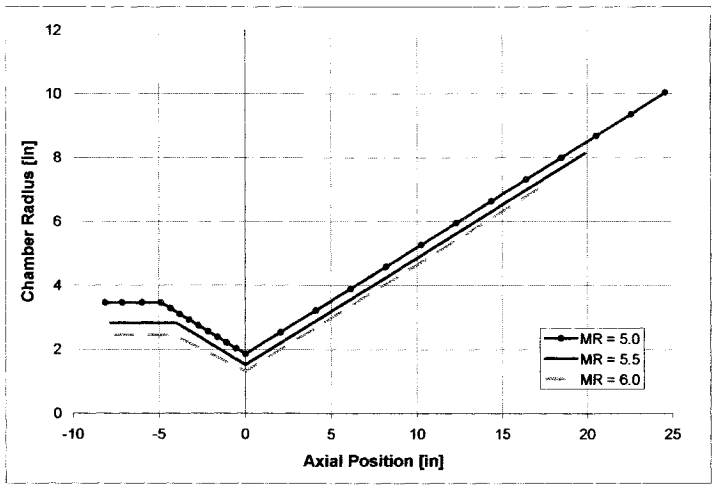

Figure 3.41. Chamber Profiles, Pc = 450 psi

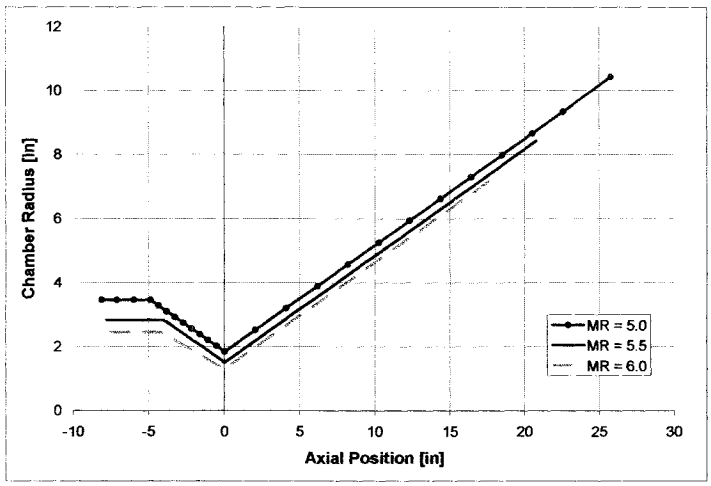

Figure 3.42. Chamber Profiles, Pc = 675 psi

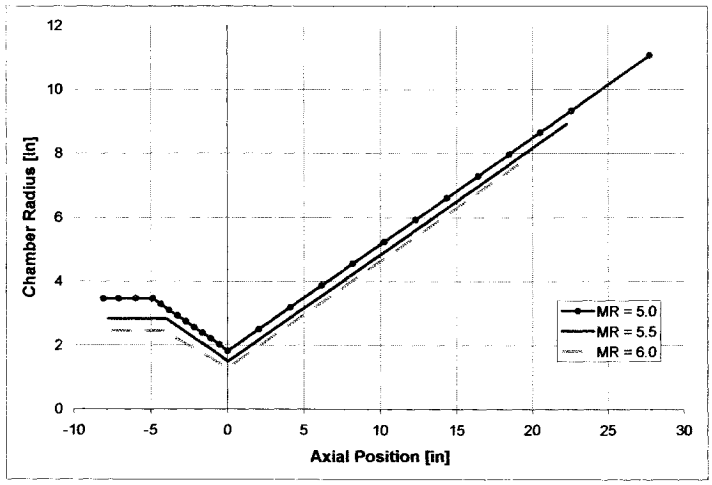

Figure 3.43. Chamber Profiles, Pc = 900 psi

Note: Recall again that in all these figures and future plots the coolant inlet is on the right and the exit on the left while the chamber inlet is on the left and nozzle exit is on the right.

As one may notice, the profiles for each of the chambers are very similar, even with the large change in chamber pressure. Although the chamber radius differs very little, the length of the chamber and nozzle varies quite a bit more.

Due to the number of input conditions that exist, there are almost an infinite number of parametric studies that could be performed by varying any number of the input parameters, including all of those listed above in Table 3.9. As mentioned previously, chamber pressure and mixture ratio were chosen as the primary variables to modify. However, as both of these parameters are varied, chamber temperature and coolant channel inlet pressure must also be modified. The new chamber temperature for each case is provided by the Cpropep code. The coolant channel inlet pressure must be manually iterated such that its value is equal to that of the chamber pressure plus the total pressure drop along the coolant channel, plus an additional fifteen percent of the chamber pressure to account for the pressure drop in the injector. One additional input that was varied was the chamber material. The primary material of choice, based on the RL10 was stainless steel, but several additional cases were also run using a copper chamber for comparison purposes. All of the variables remained the same with the two different chamber materials except for the coolant inlet pressure which had to be manually reconverged based on the new temperature restrictions of copper. The table below summarizes all of the input parameters that vary with each of the different chamber pressures, mixture ratios, and materials that were chosen:

Table 3.10. Design Trade Study Variable Input Parameters

Procedure Parameters	Value									Units
Chamber Pressure (Pc)	450			675			900			psi
Mixture Ratio (MR)	5.0	5.5	6.0	5.0	5.5	6.0	5.0	5.5	6.0	n/a
Chamber Temperature	5805.6	5987.9	6118.0	5863.3	6059.6	6201.6	5902.1	6108.8	6259.7	Rankine
Total Coolant Mass Flow Rate	3.348	3.091	2.870	3.348	3.091	2.870	3.348	3.091	2.870	lbm/s
Coolant Inlet Static Pressure (Stainless Steel)	627.5	634.5	644.5	1061.5	1084.2	1162.0	1698.0	1717.0	n/a	psi
Coolant Inlet Static Pressure (Copper)	556.0	560.0	568.0	874.0	870.0	874.0	1285.7	1222.4	n/a	psi
Chamber & Nozzle Length	32.70	27.69	24.78	33.89	28.60	25.50	35.84	30.07	26.70	inches

The values missing from the table for the inlet pressure at a chamber pressure of 900 psi and a mixture ratio of 6.0 for both chamber materials are absent due to the fact that convergence could not be achieved in this more extreme case, demonstrating the limitations of the parabolic marching algorithm. Although chamber pressures higher than 900 psi have been run in previous verification cases, the combination of the other input parameters being used resulted in a flow regime outside the procedures capability.

The results that are of primary interest in this study are the hot-wall side temperature distribution, the geometry of the coolant channel generated by the procedure, and the total pressure loss and heat pickup per channel. The temperature and geometry results have been plotted as a function of chamber axial position at a constant chamber pressure with different mixture ratios and at a constant mixture ratio at varying chamber pressures. The total pressure loss and heat pick up are plotted as functions of chamber pressure at varying mixture ratios. The results for the stainless steel chamber will be discussed first followed by the copper chamber.

3.2.2 Stainless Steel Chamber Design

The first set of six plots display the hot-wall side temperature trends in each of the viable eight chambers that were designed:

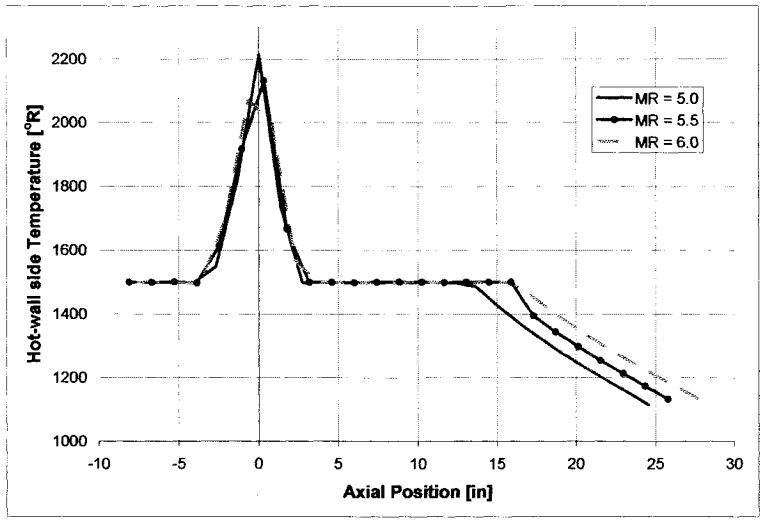

Figure 3.44. Hot-Wall Side Temperature Distribution, Pc = 450 psi

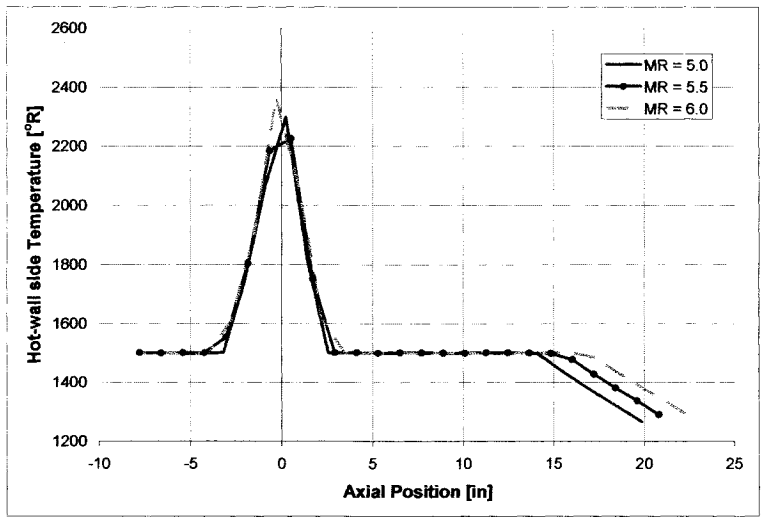

Figure 3.45. Hot-Wall Side Temperature Distribution, Pc = 675 psi

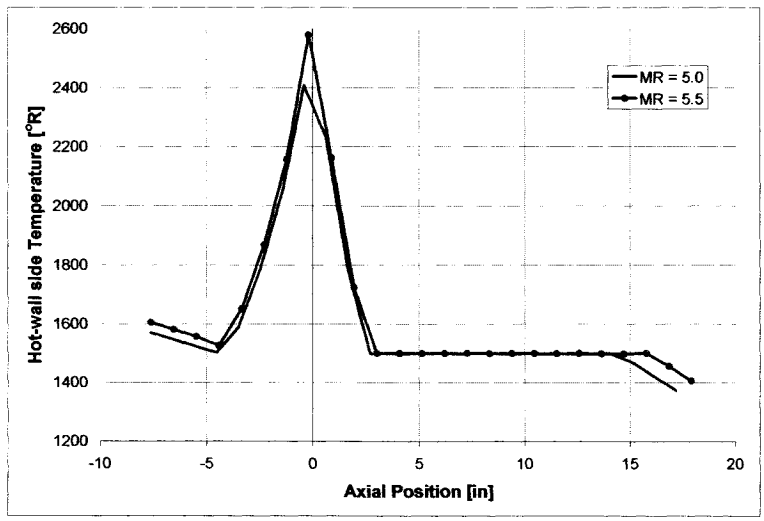

Figure 3.46. Hot-Wall Side Temperature Distribution, Pc = 900 psi

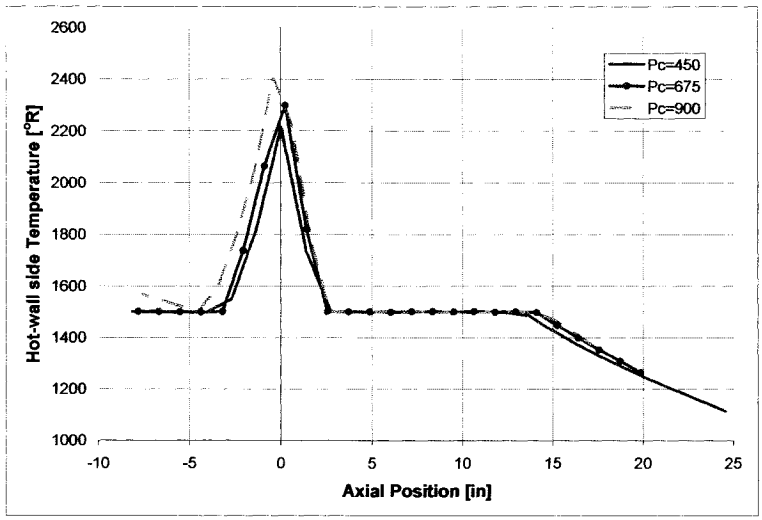

Figure 3.47. Hot-Wall Side Temperature Distribution, MR = 5.0

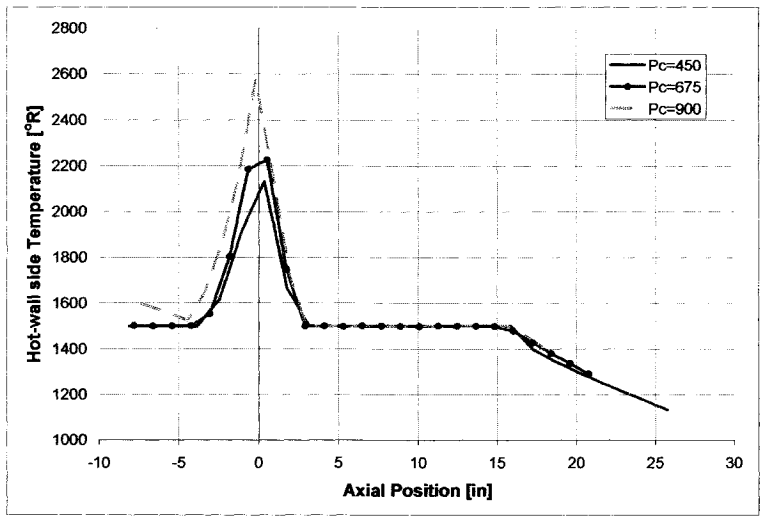

Figure 3.48. Hot-Wall Side Temperature Distribution, MR = 5.5

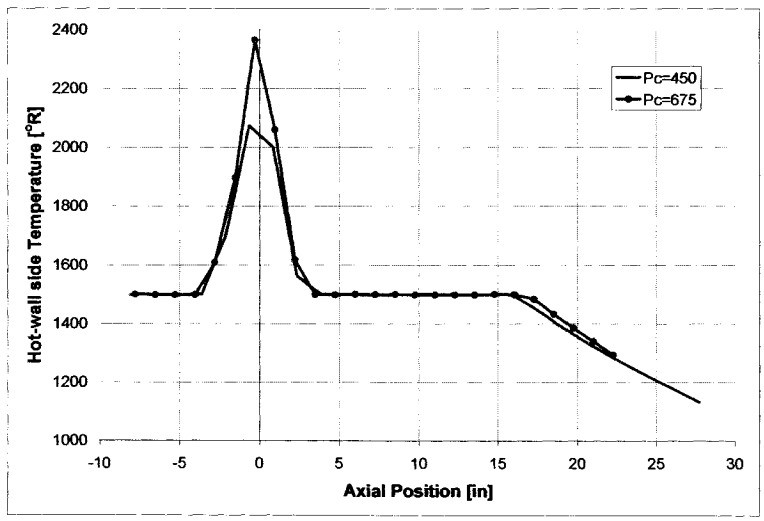

Figure 3.49. Hot-Wall Side Temperature Distribution, MR = 6.0

The first important feature to take note of when examining these plots is the region of constant temperature typically present upstream and downstream of the throat (denoted by an axial position of zero). The chosen hot-wall side temperature design point for all of these cases was 1500 °R, based on the maximum value used in the original RL10 study. It is clear from the figures that the design procedure was not able to successfully hold the wall temperature at this value due to reaching one of the several constraints placed on the coolant channel geometry. In the nozzle (denoted by positive axial position values), particularly close to the exit where the area is greatest, the wall is much cooler than the rest of the chamber. Thus, the design routine, in an attempt to raise the temperature to the design point, increases the height of the coolant channels to their maximum allowed value. Even at this level though, the wall temperature in the nozzle is still often well below the design point. As the nozzle area continues to decrease as the throat is approached, the temperature is successfully held at 1500 °R. When the area reaches a minimum at the throat, the maximum coolant flow Mach number is typically reached and although the chamber is too hot, there is no additional height modification that the design routine can perform to decrease the wall temperature. Upstream of the throat (denoted by negative axial position values), as the coolant channels pass through the convergent cone section and the constant area barrel section of the chamber, the routine is typically able to hold the design temperature for most of the cases.

Looking now at the overall trends in the first set of three plots, lower chamber pressure clearly results in lower hot wall temperatures although this still creates problems holding the design temperature in the nozzle region. Similarly, lower mixture ratios also result in lower hot wall temperature as apparent primarily in the nozzle region. At the

throat, this trend does not always appear to hold true. This is because the coolant channels are broken up into uniformly sized and distributed control volumes. Given the different lengths of the chambers, a data point is not always guaranteed to lie directly at the throat. In addition, the maximum Mach number constraint is being exceeded at this point. In order to rectify this, the design routine must increase the height in small increments until the Mach number is less than 0.3, which results in slightly different values for each test case. In the next set of three plots where mixture ratio is held constant, these same trends are validated with an increase in chamber pressure and mixture ratio both leading to an increase in hot wall temperature. All of these plots demonstrate that the current design for the engine may result in problems at the throat although the maximum temperatures are still several hundred degrees below the melting point of stainless steel. To reduce the temperature spike at the throat, numerous steps could be taken including relaxing some of the design constraints if possible or, in a more drastic approach, altering some of the other variables that have remained fixed such as the number of coolant channels or the wall thickness in the throat region.

The next set of six figures depicts the coolant channel height profile generated by the design procedure in its attempt to hold the hot-wall side temperature at the constant prescribed value. Each of these figures correspond directly to one of the six hot-wall side temperature plots just discussed:

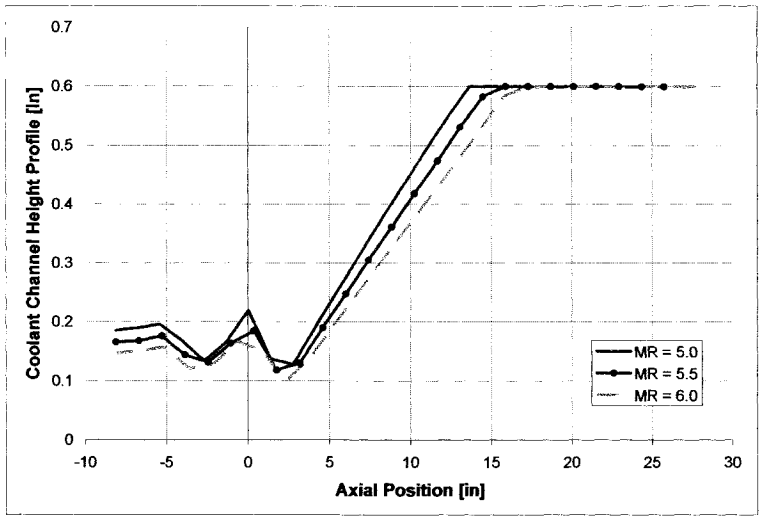

Figure 3.50. Coolant Channel Height Profile, Pc = 450 psi

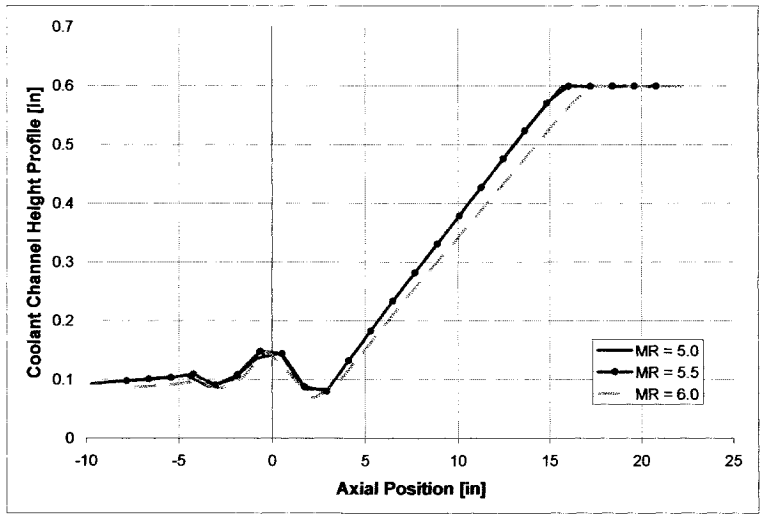

Figure 3.51. Coolant Channel Height Profile, Pc = 675 psi

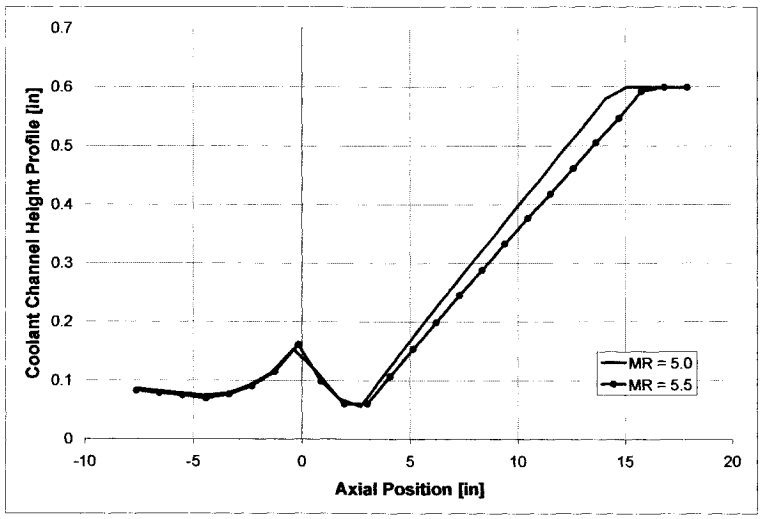

Figure 3.52. Coolant Channel Height Profile, Pc = 900 psi

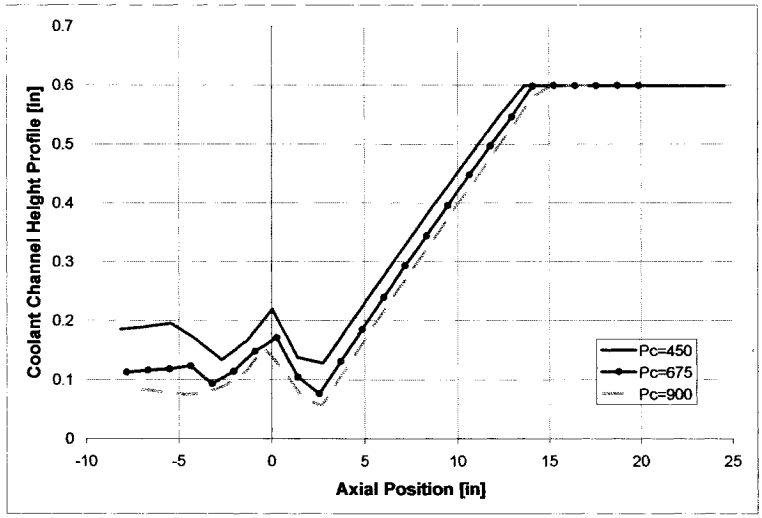

Figure 3.53. Coolant Channel Height Profile, MR = 5.0

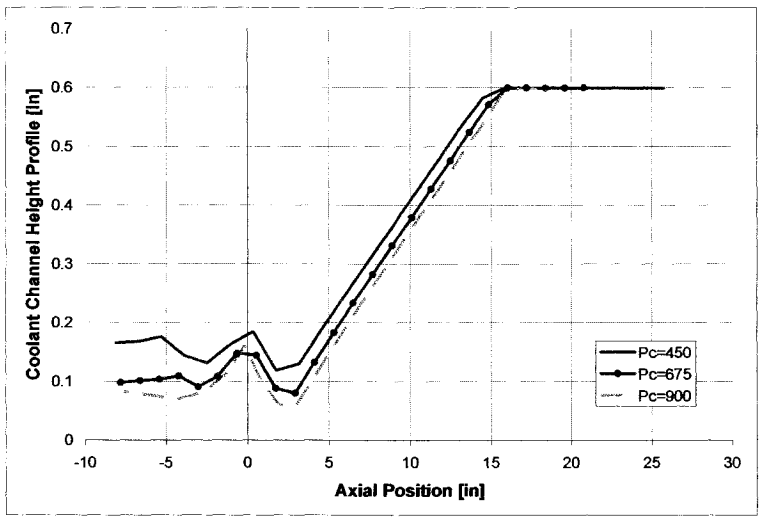

Figure 3.54. Coolant Channel Height Profile, MR = 5.5

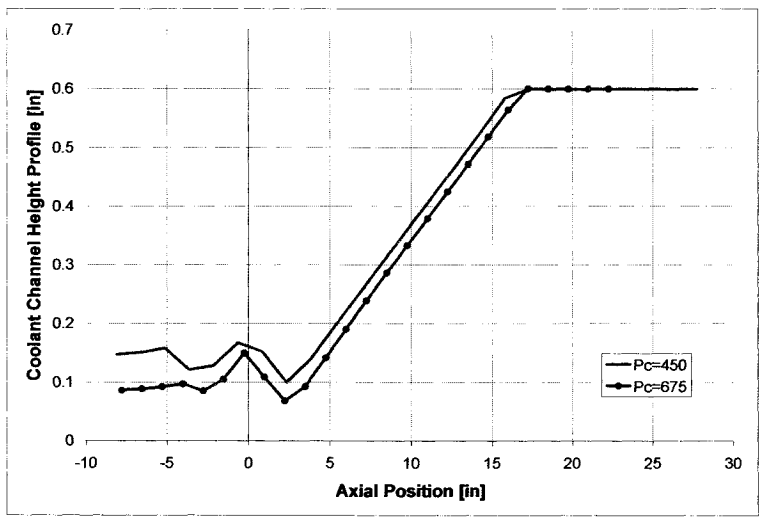

Figure 3.55. Coolant Channel Height Profile, MR = 6.0

It is very evident in each of the figures that in the nozzle region the coolant channel heights are at their maximum allowed value of 0.6 inches. Again, once the nozzle area begins to decrease more significantly, the coolant channel heights are no longer violating any constraints and are able to hold the design temperature until the throat region. At this point typically either the maximum Mach number or maximum aspect ratio constraints are reached and the design routine is forced to accept a higher wall temperature.

Looking at the trends in the first set of figures, it appears that mixture ratio does not have a significant effect on the height profile as compared to chamber pressure when looking at the second set of figures. As expected, lower chamber pressures, and to some extent lower mixture ratios, result in higher coolant channel heights. Larger heights result in decreased flow velocity and thus higher temperatures and less cooling. As mentioned previously when examining the hot-wall side temperature distributions, lower chamber pressures and mixture ratios result in lower temperatures and thus, less cooling and correspondingly higher coolant channel heights are needed. On a final note, the height profile is clearly somewhat jagged in the throat region and would obviously require some smoothing before final design and fabrication. However these plots provide a valuable foundation for preliminary design work and at the very least establish a base geometry range for the coolant channel height profile.

The final set of six figures shows the coolant channel area distribution determined by the previously displayed height profiles and the coolant channel width distribution. A constant land width of 0.03 inches was chosen which resulted in a variable width distribution based on the chosen number of coolant channels and the perimeter of the chamber at each axial location:

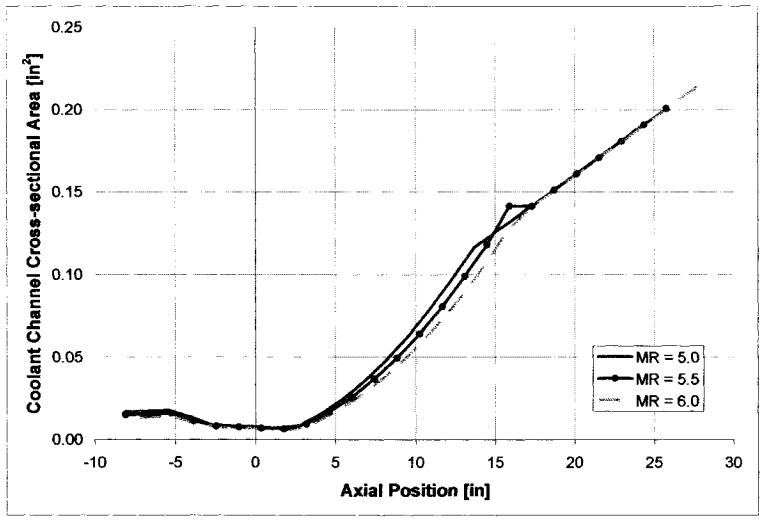

Figure 3.56. Coolant Channel Area Distribution, Pc = 450 psi

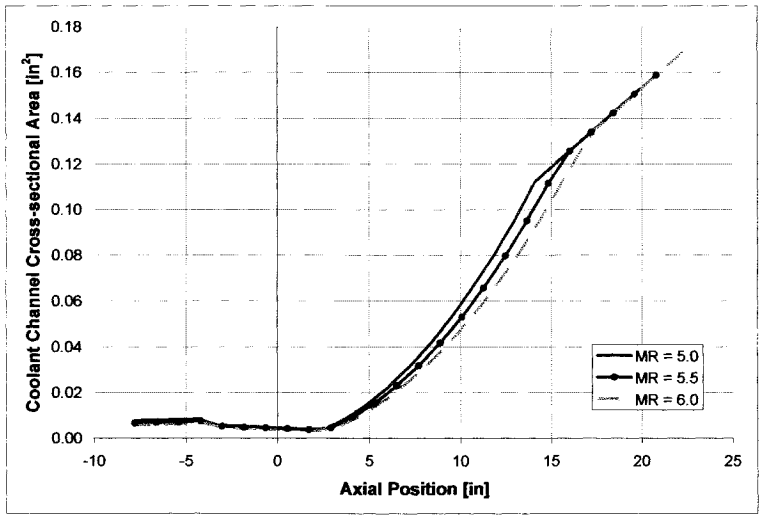

Figure 3.57. Coolant Channel Area Distribution, Pc = 675 psi

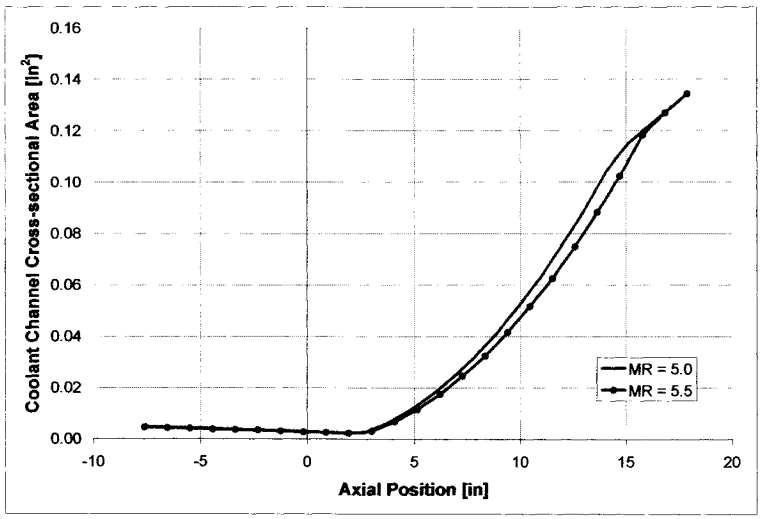

Figure 3.58. Coolant Channel Area Distribution, Pc = 900 psi

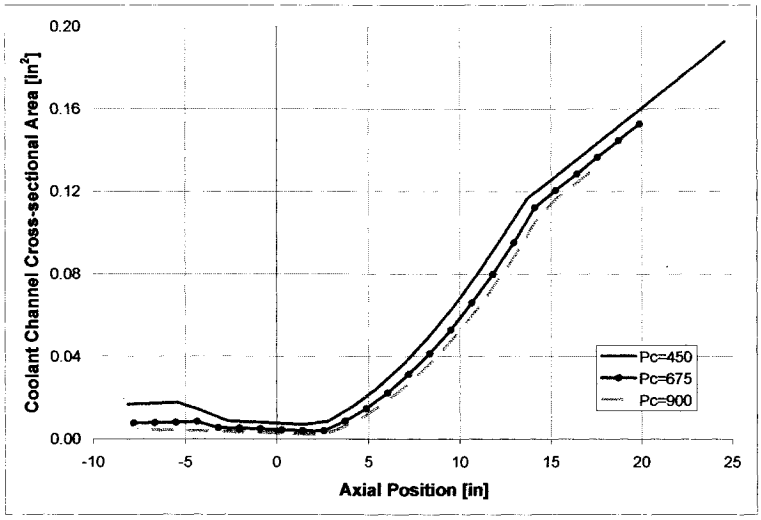

Figure 3.59. Coolant Channel Area Distribution, MR = 5.0

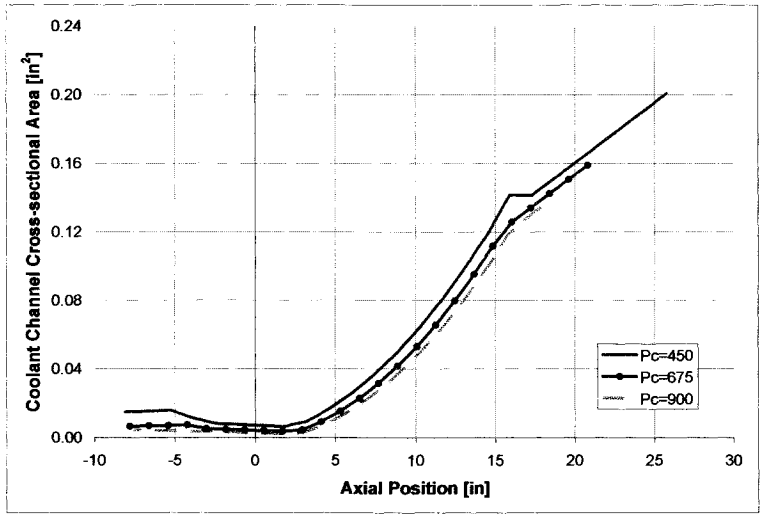

Figure 3.60. Coolant Channel Area Distribution, MR = 5.5

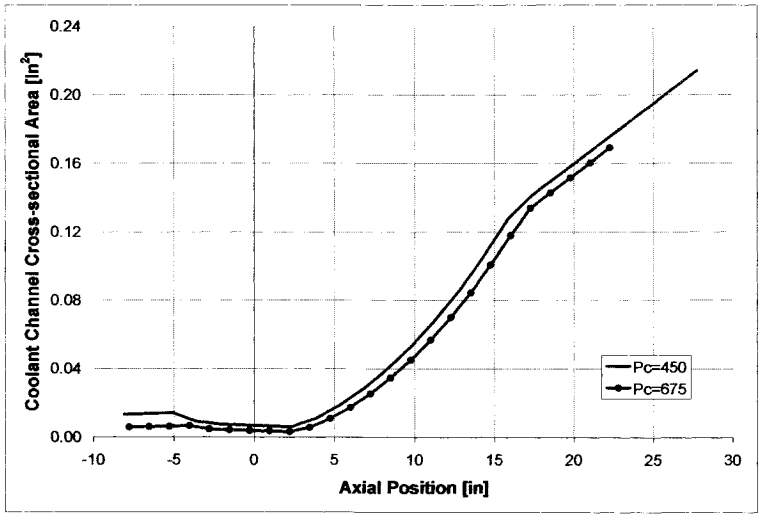

Figure 3.61. Coolant Channel Area Distribution, MR = 6.0

Due to the variable coolant channel width distribution, the area distribution is much smoother than the height profiles shown in Figure 3.50 - Figure 3.55, although the general trend is obviously very similar. It is no surprise either that the area distribution closely mirrors the shape of the chamber contour as would be expected. Once again it appears that the chamber pressure has a larger impact on the area distribution compared to the mixture ratio. In addition, as with the height profiles, the larger area distributions correspond to lower mixture ratios and lower pressures. As an alternative to holding the coolant channel land width constant, a tradeoff between coolant channel height and width could possibly be made in order to smooth out the height profile while maintaining the same area distribution.

The final two plots of interest depict the total pressure loss and the total heat pickup along the entire coolant channel as a function of chamber pressure. These two variables are important metrics in the rocket industry for gauging the performance of a regenerative cooling jacket and are shown here for all of the design cases run so far:

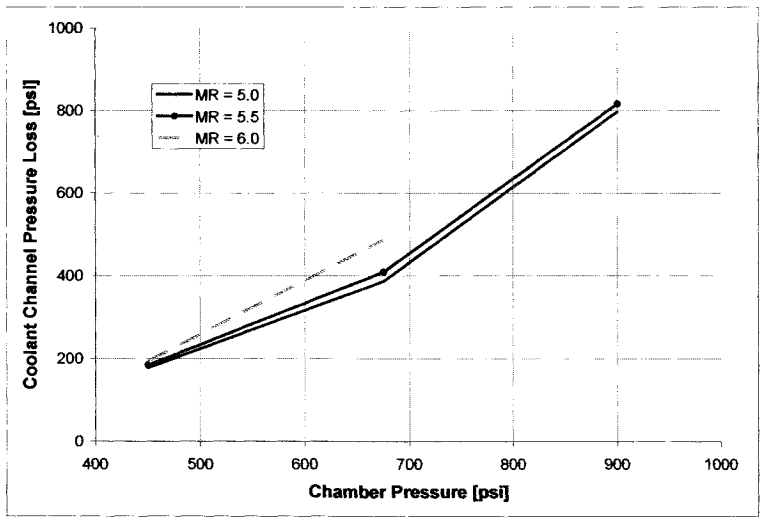

Figure 3.62. Coolant Channel Total Pressure Loss (ΔP)

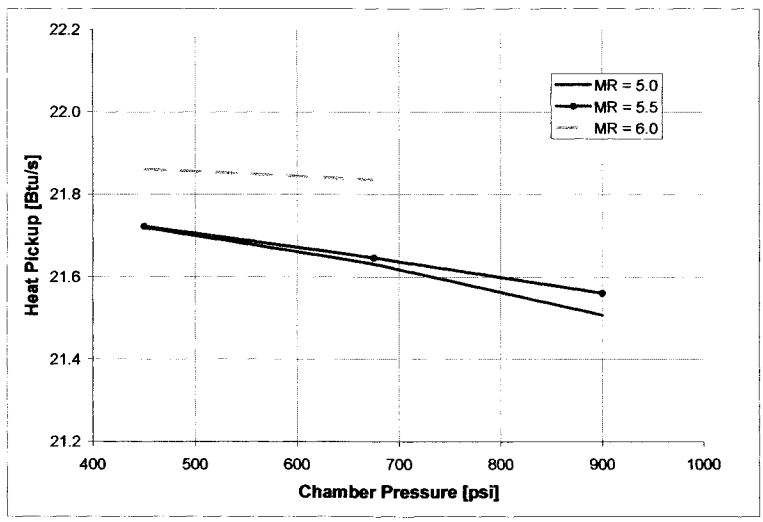

Figure 3.63. Coolant Channel Total Heat Pickup

Although it is difficult to make any overarching comments about the trends shown in these figures given that there are only a few data points, there are several obvious conclusions that can be made. There is no question that as the chamber pressure is increased, the coolant inlet temperature must also increase which in turn results in greater pressure loss in the coolant channels. Based on Figure 3.62, increasing the mixture ratio also increases the pressure loss as well but not by any drastic measures. In regards to the total heat pickup shown in Figure 3.63, lower pressures result in higher levels of heat

transfer to the coolant while lower mixture ratios have the opposite effect. Typically there is a tradeoff between maximizing total heat pickup and minimizing pressure loss in order to ensure the most efficient regenerative cooling design in an expander cycle engine. In this case, based on the results and trends presented in these two figures, it appears that lower chamber pressures and moderate to high mixture ratios would be the optimal compromise.

3.2.2.1 Chamber Barrel Length Study

Another simple design modification that was tested for a single design case was the effect of increasing the chamber barrel length. The chamber barrel refers to the constant diameter section of the chamber upstream of the convergent cones section of the throat. Often increasing this length can improve the efficiency of the regenerative cooling jacket by increasing the amount of heat pickup in the channels. However, this does not come without a penalty given that a longer chamber results in increased weight and longer coolant channels mean greater pressure losses. In order to quantify these trends, the second design chamber with a mixture ratio of 5.5 and a chamber pressure of 675 psi was chosen as the test chamber. The barrel length for this chamber was calculated to be approximately 3.83 inches. This length was first increased by 50% and then 100%, resulting in new barrel lengths of approximately 5.75 inches and 7.66 inches, and the design case was rerun with these new values. The resultant hot-wall side temperature distribution as well as the height profile and area distribution remained almost identical to the initial case. However, a distinct impact on the coolant channel total pressure loss and heat pick was seen as expected and is shown in the following two figures:

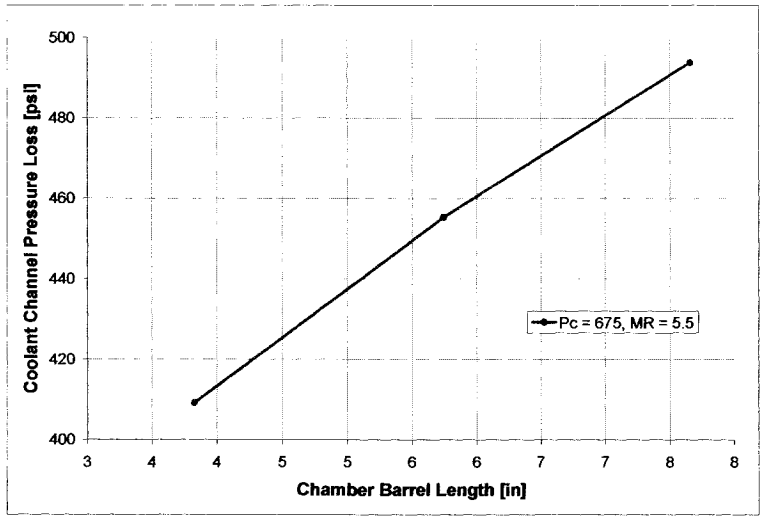

Figure 3.64. Chamber Barrel Length Effect on Total Pressure Loss

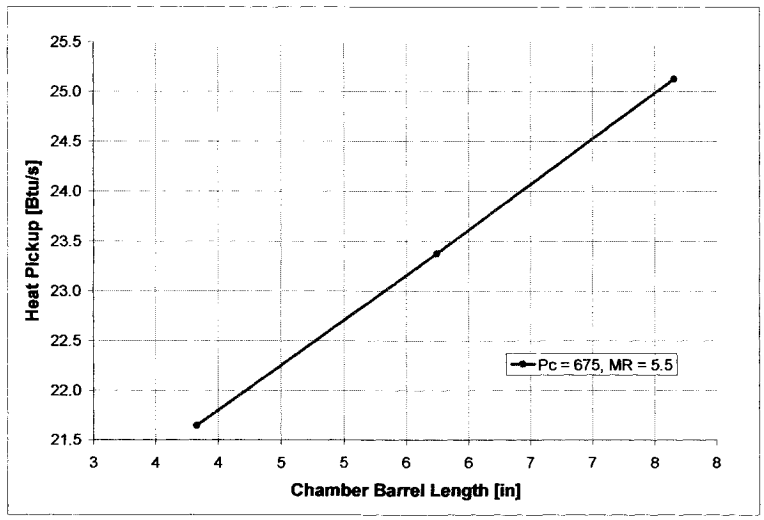

Figure 3.65. Chamber Barrel Length Effect on Total Heat Pickup

The effect of increasing the chamber barrel length has a virtually linear effect on the total pressure loss and heat pick up. Doubling the barrel length in this case increases the pressure loss by about 20% and increases the heat pick up by approximately 16%. As mentioned previously, increasing the heat pick up is beneficial but increasing the pressure drop and the weight of the engine is clearly not. In this case the tradeoff does appear to be worthwhile. However a more detailed study taking into account other factors would need to be performed before any final decision was made.

3.2.3 Copper Chamber Design

As mentioned previously, the same design cases that were run with stainless steel chambers were also run using copper chambers in an identical fashion. Although the chamber geometries remain the same, the coolant inlet pressures used are different due to the lower maximum prescribed hot wall temperature required due to copper's lower melting point. Instead of designing the chamber to a temperature of 1500 ^{o}R, the copper chambers were design to a temperature of 1200 ^{o}R based on another RL10 trade study report[7]. Once again, the first set of six plots depicts the hot-wall side temperature distribution for all eight copper chambers as a function of coolant channel axial position:

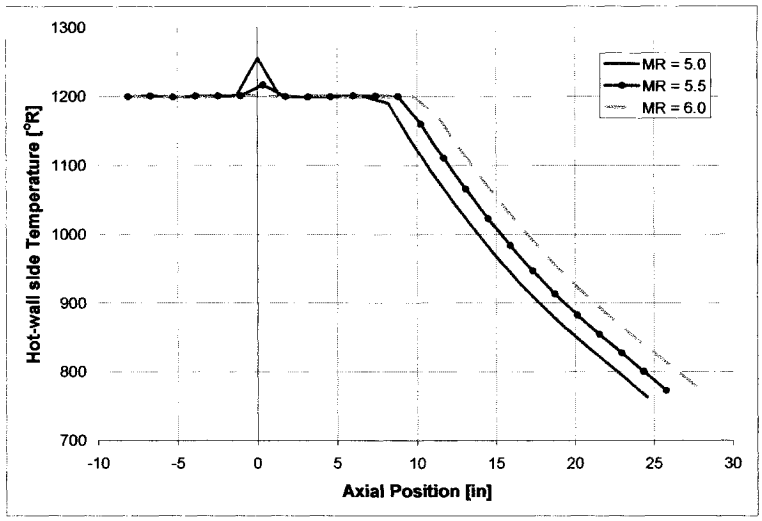

Figure 3.66. Hot-Wall Side Temperature Distribution, Pc = 450 psi

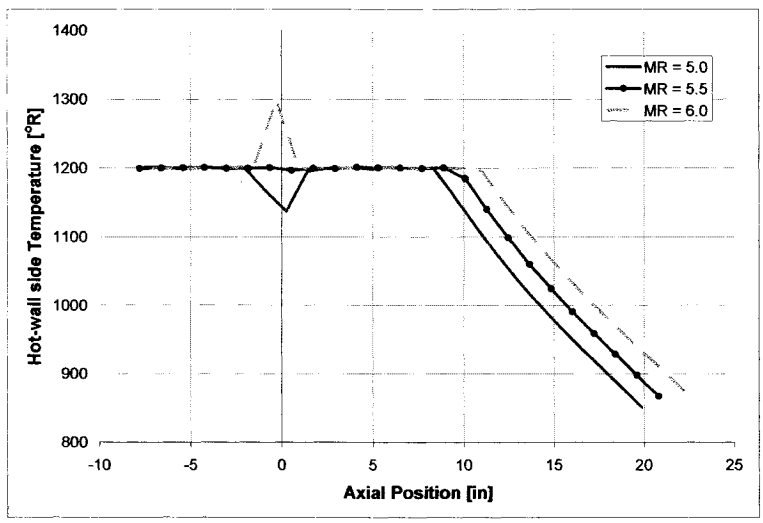

Figure 3.67. Hot-Wall Side Temperature Distribution, Pc = 675 psi

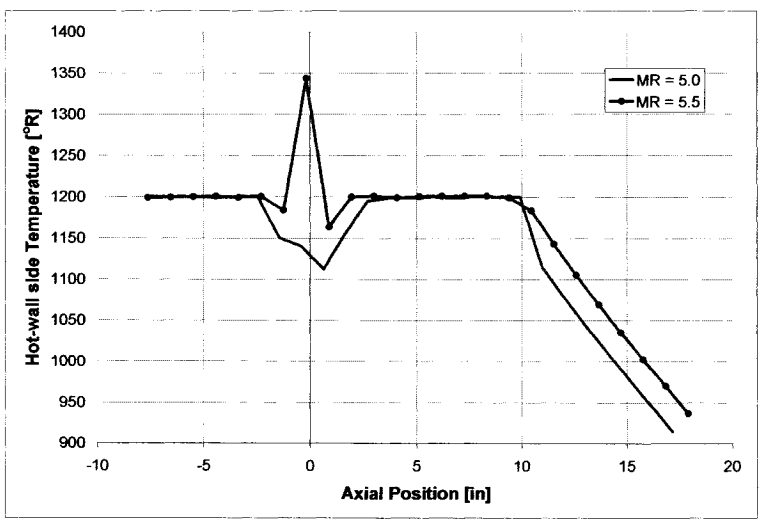

Figure 3.68. Hot-Wall Side Temperature Distribution, Pc = 900 psi

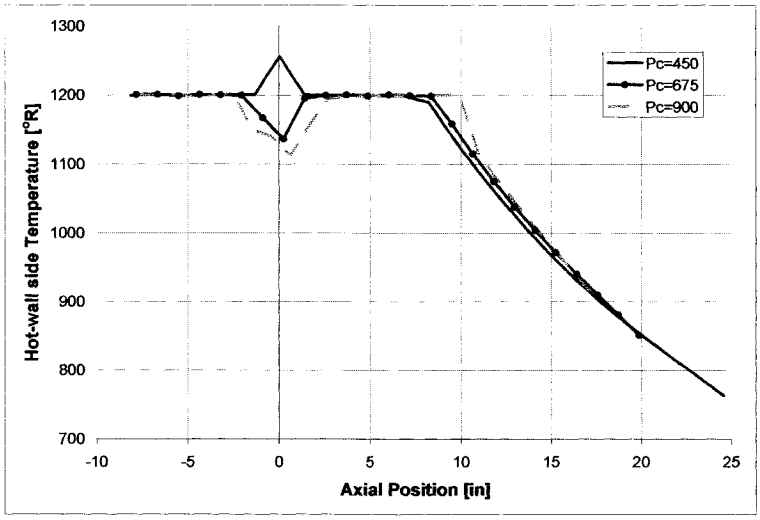

Figure 3.69. Hot-Wall Side Temperature Distribution, MR = 5.0

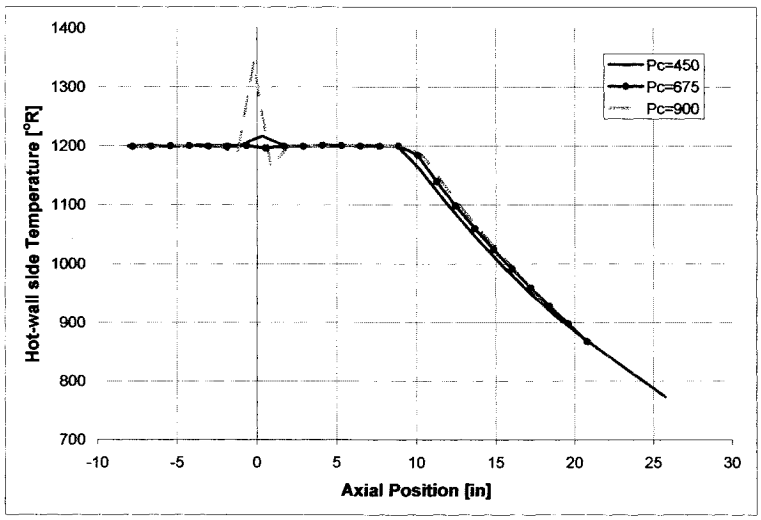

Figure 3.70. Hot-Wall Side Temperature Distribution, MR = 5.5

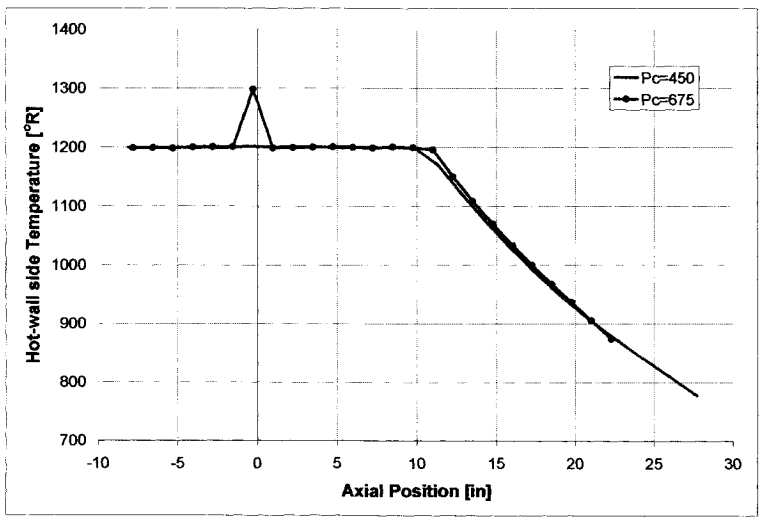

Figure 3.71. Hot-Wall Side Temperature Distribution, MR = 6.0

Due to copper's higher thermal conductivity, it is very evident from the plots that the design routine is able to prevent the large temperature spikes at the throat seen in many of the stainless steel chambers. However, the trade off is that the coolant channel heights reach the maximum value in the nozzle section over a much greater length and the design temperature can not be achieved. If it is not a problem that the nozzle is cooler than the design temperature, then this is not an issue. There are several instances where the throat is actually cooler than the design temperature, which again means that one of the design constraints is being reached. In these instances, the constraint is typically the maximum aspect ratio of six as opposed to the maximum Mach number constraint that was usually the issue in the stainless steel chambers. The overall trends in the figures again remain the same with lower mixture ratios and chamber pressures corresponding to lower wall temperatures. Although these chambers would seem much better from a temperature stand point, copper by itself is not commonly used as a chamber material due to fabrication and structural issues and is usually alloyed with other metals. However, these plots clearly suggest that it may be worth spending the extra time and funds to design a copper alloy chamber since there are definite improvements for regenerative cooling due to its high thermal conductivity.

As with the stainless steel design study, the next set of six plots depicts the coolant channel height profile that was chosen by the design routine to maintain the chamber at the new design temperature:

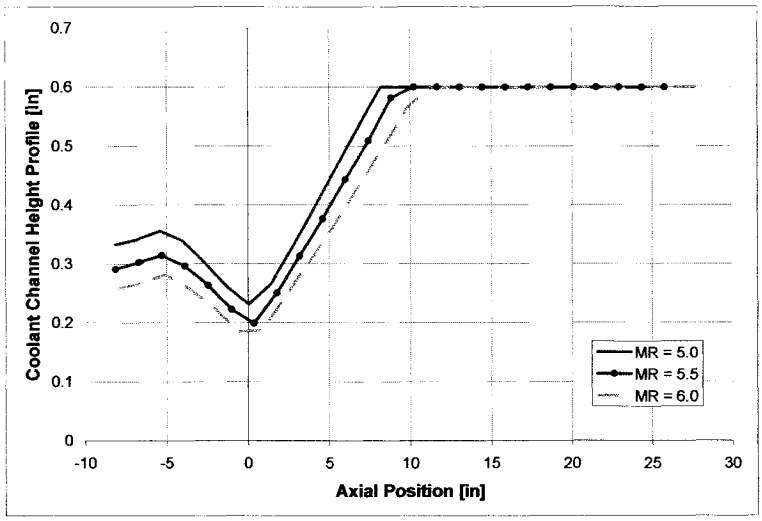

Figure 3.72. Coolant Channel Height Profile, Pc = 450 psi

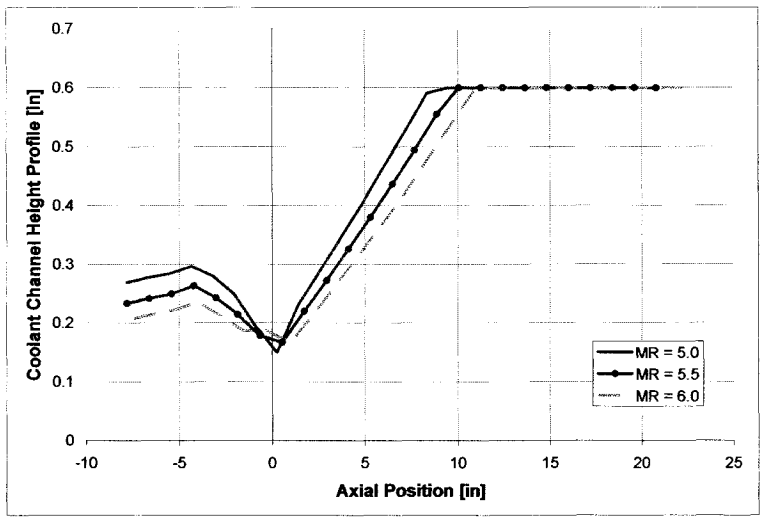

Figure 3.73. Coolant Channel Height Profile, Pc = 675 psi

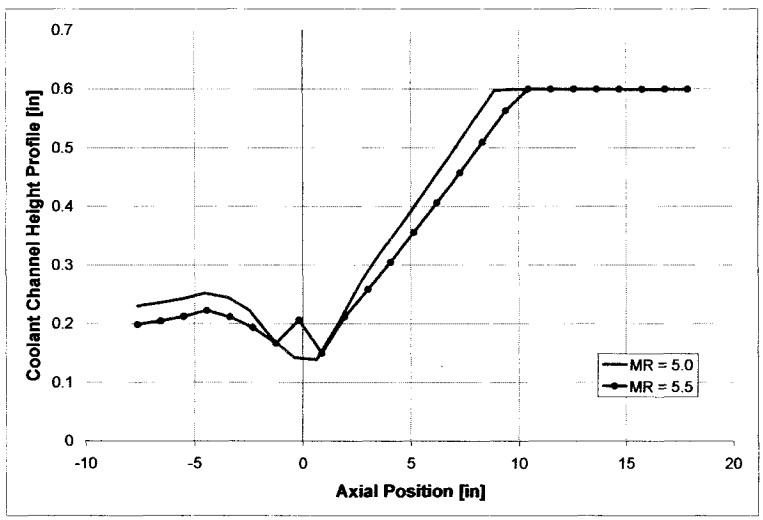

Figure 3.74. Coolant Channel Height Profile, Pc = 900 psi

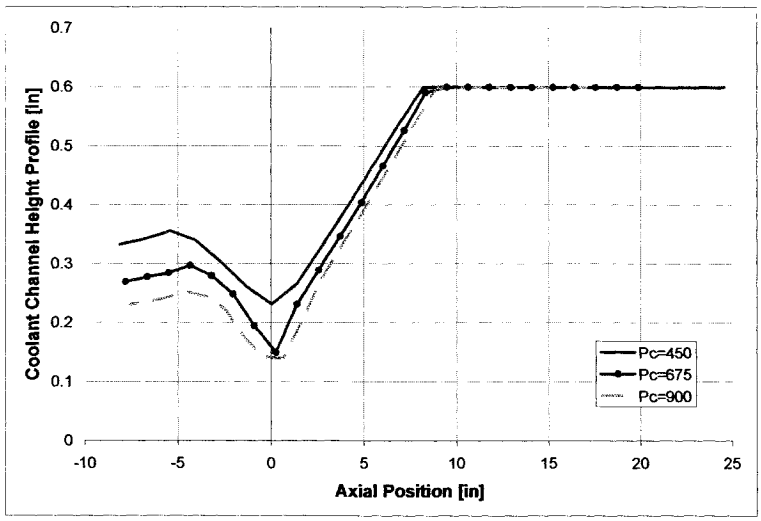

Figure 3.75. Coolant Channel Height Profile, MR = 5.0

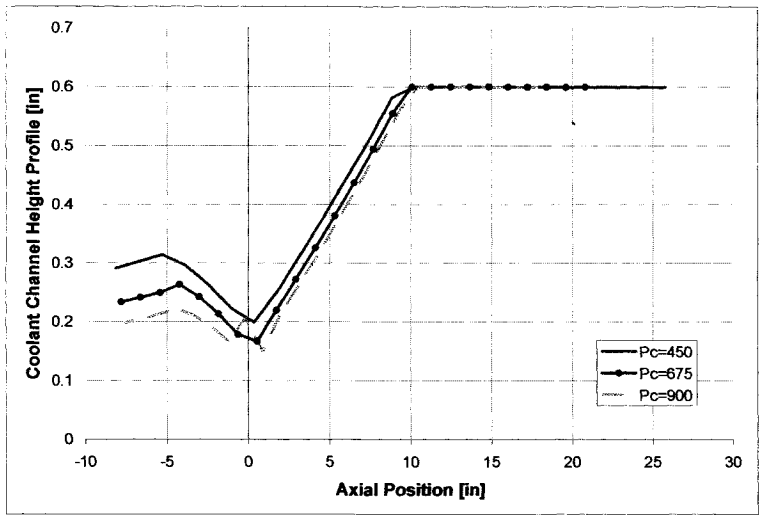

Figure 3.76. Coolant Channel Height Profile, MR = 5.5

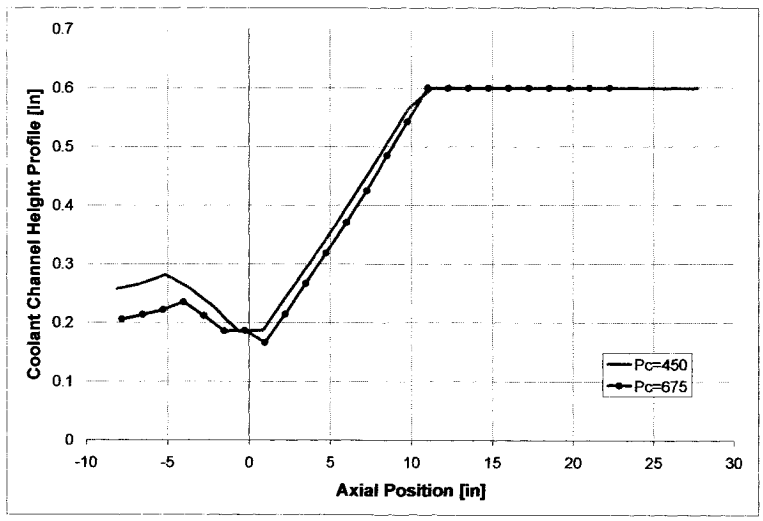

Figure 3.77. Coolant Channel Height Profile, MR = 6.0

It is immediately obvious that these height profiles are much smoother than the ones designed with the stainless steel chambers given the absence of the large temperature spike in the throat region. The effect that chamber pressure and mixture have on the profile is also much clearer in these figures, especially at lower chamber pressures and mixture ratios. At higher chamber pressure and mixture ratios, the curves lie much closer to each other as opposed to the distributions at lower values. Again the lower values also typically correspond with the greater height values as well.

Once again, it is important to examine the coolant channel area distributions as well which are determined using the height and width distributions. The channel width distributions for the copper chambers are also calculated by fixing the land widths at a constant value 0.3 inches again and letting the chamber perimeter and number of coolant channels determine the resultant width:

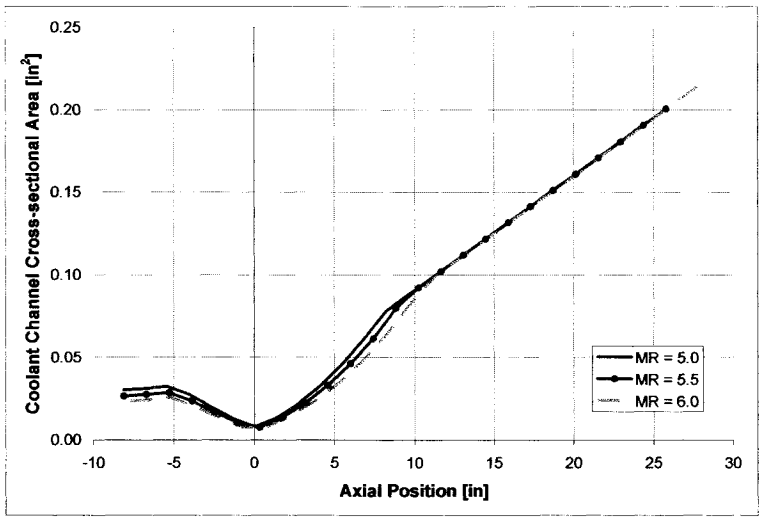

Figure 3.78. Coolant Channel Area Distribution, Pc = 450 psi

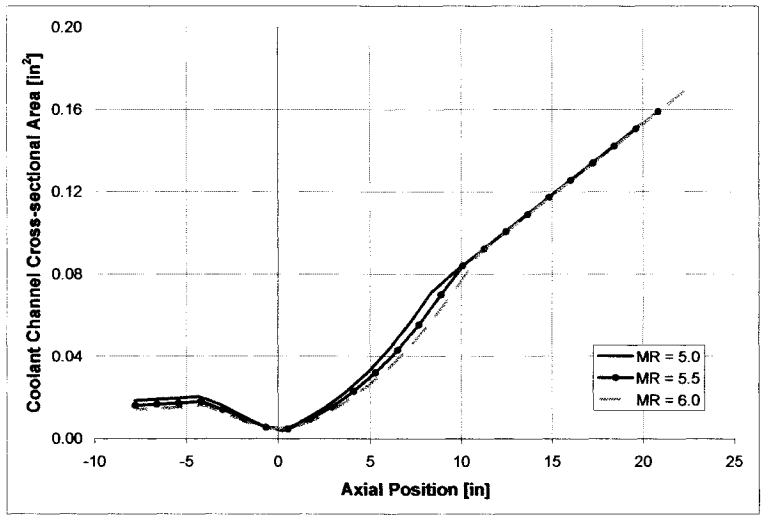

Figure 3.79. Coolant Channel Area Distribution, Pc = 675 psi

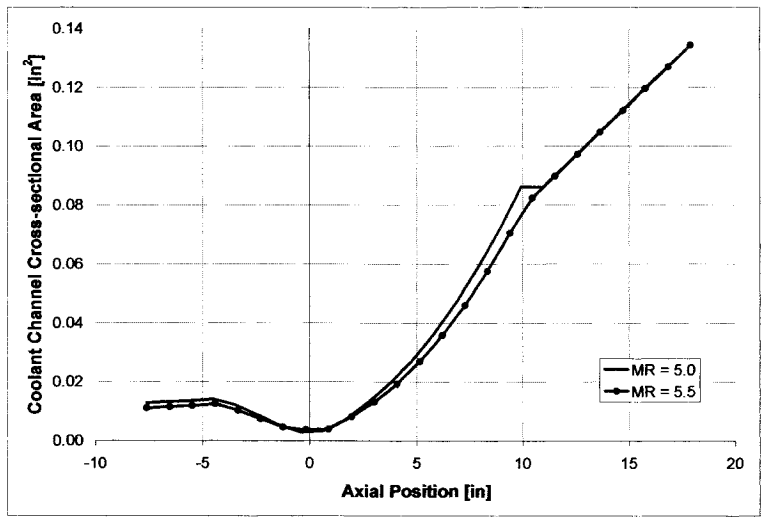

Figure 3.80. Coolant Channel Area Distribution, Pc = 900 psi

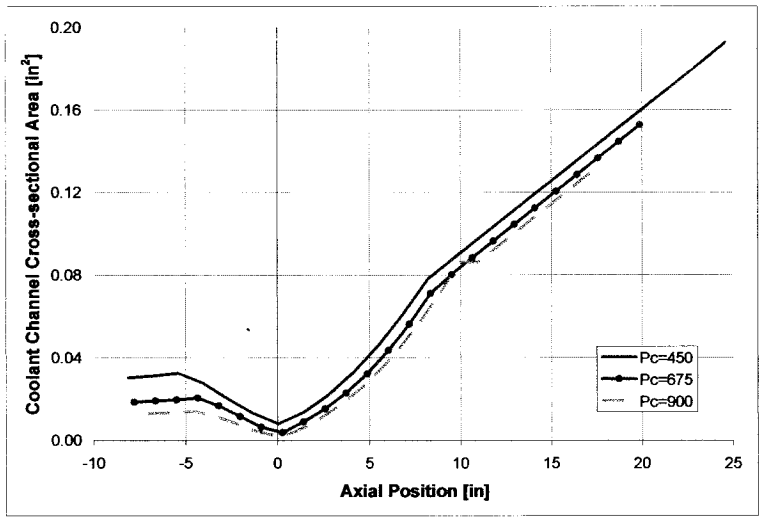

Figure 3.81. Coolant Channel Area Distribution, MR = 5.0

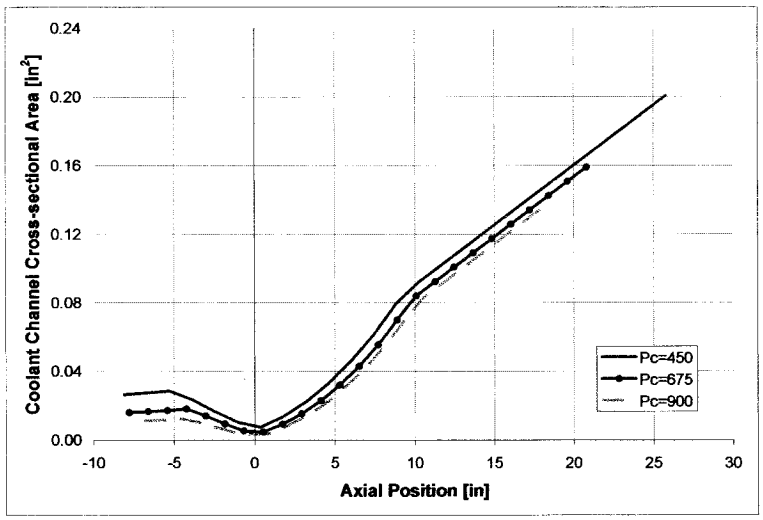

Figure 3.82. Coolant Channel Area Distribution, MR = 5.5

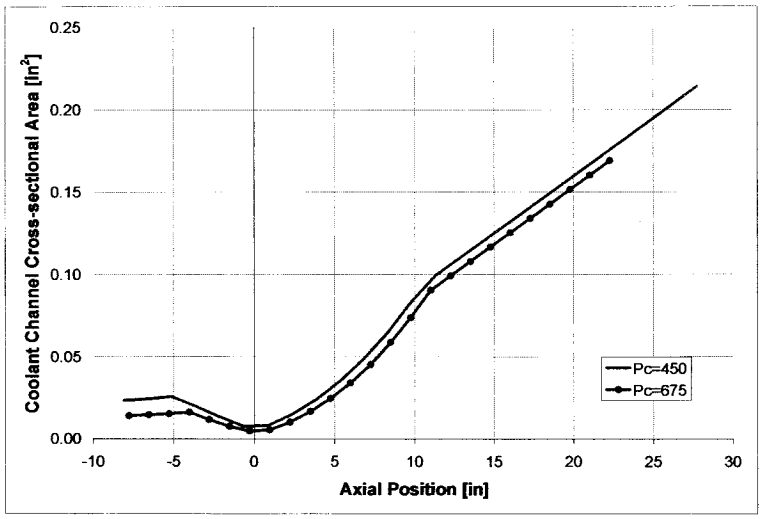

Figure 3.83. Coolant Channel Area Distribution, MR = 6.0

As expected, the area distributions are much smoother and tend to be effected more by chamber pressure than mixture ratio, especially at lower pressures, as was observed in the stainless steel chambers. Although the shape of the distributions overall are very similar to the stainless steel chambers, the magnitude of the area tends to be slightly higher, primarily in the throat region and upstream. This is probably directly related to the fact that the copper chambers do not have the same cooling issues that the stainless steel chambers did and thus the coolant channels can be slight larger, providing less cooling.

Finally, it is important to examine the primary coolant channel metrics, total pressure loss and heat pickup, shown in Figure 3.84 and Figure 3.85:

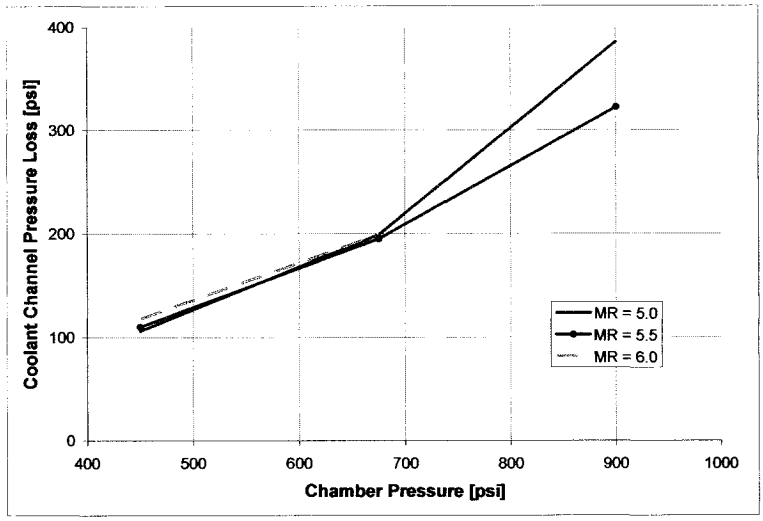

Figure 3.84. Coolant Channel Total Pressure Loss (ΔP)

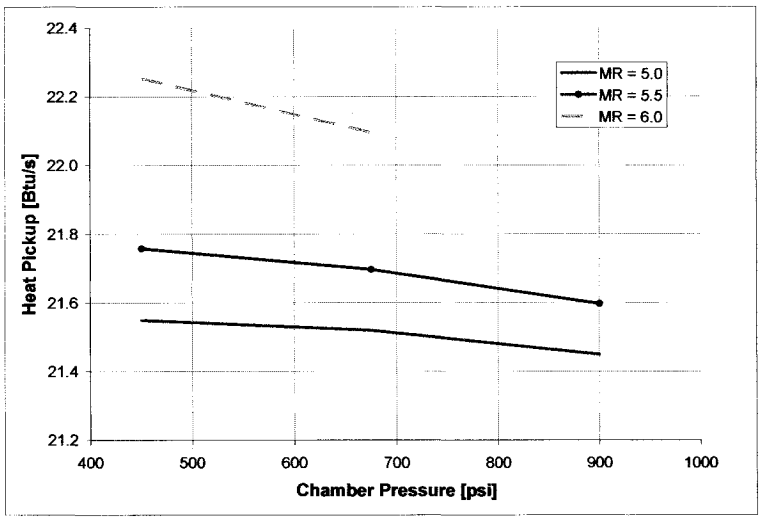

Figure 3.85. Coolant Channel Total Heat Pickup

The trends are again similar to that of the stainless steel chambers, with an increase in chamber pressure resulting in greater pressure losses and lower levels of heat pickup. However, the magnitude of the total pressure lost is drastically different. In the stainless steel chambers, the pressure loss values varied from around 200 psi all the way up to 800 psi. In the copper chamber, the pressure losses range from only 100 psi to around 400 psi, essentially half that of stainless steel. On the other hand, the heat pickup trends are relatively similar in magnitude although the curves are spaced out a bit more with the

higher mixture ratio levels now providing slightly more heat transfer and the lower mixture ratio actually providing slightly less. Thus, it would appear in this case that a mixture ratio of 5.5 is probably a good compromise and that lower pressures are again more favorable. Given that the pressure losses are much smaller with the copper chamber, a situation like this might benefit from lengthening the chamber barrel length unlike the case that was examined with the stainless steel chamber.

With the completion of the design trade study, it is difficult to make any profound decisions about which chamber pressure, mixture ratio and chamber material without performing more exhaustive studies and research. However, fundamental knowledge of the important trends in the coolant channel design has been gained and there is a clear understanding of where future investigations should focus their efforts. The copper chambers clearly have some important advantages over the stainless steel chambers and lower pressures and moderate mixture ratios appear to generate the best results. However, these trends only take into account a few basic metrics and by no means address other important structural concerns and efficiency issues associated with these variables. Once again, further investigations would need to be performed to make the final decisions but the results presented here provide an important foundation for making preliminary decisions that will affect all of the future work.

4. Conclusion

With the completion of this study, numerous conclusions may be drawn from the material presented and several areas for future and more extensive research have been illuminated. The procedure that has been developed has successfully met its primary goal of efficiently and accurately designing the coolant channel height profile for a liquid rocket engine to meet a specified uniform hot wall temperature. In addition, it can quickly analyze an existing coolant channel design and provide the user with all of the important fluid variables along the entire length of the cooling jacket. Overall, the procedure has demonstrated a drastically reduced analysis solution time compared to the Linesolve fluid solver and the capability for running each of its design cases in less than five minutes. It also has incorporated numerous features that expand its flexibility, not all of which have been utilized to their full potential in the design trade study, including alternative fuels, multiple wall layers of varying materials and thickness and a basic structural and thermal stress analysis. The control volume marching technique when applied to coolant channel design, although very fast, clearly has some stability issues, especially when more complex fluid regimes and geometries are tackled. There are definitely more opportunities for expanding the research of this technique and improving its stability. Hopefully future studies can undertake some of these issues and continue to provide new efficient procedures in this area of research for the rocket industry.

References

[1] Avallone, E.A., Bumeister III, T., "Marks' Standard Handbook for Mechanical Engineers," 10th Ed., McGraw-Hill Co., Inc., New York, 1996.

[2] Binder, M., Tomsik, T., Veres, J.P., "RL10A-3-3A Rocket Engine Modeling Project," NASA TM-107318, 1997.

[3] Campbell, Bryan T. Private discussions. November 2007 – June 2009.

[4] Davis, R. L. and Campbell, B. T , "Quasi-1D Unsteady Flow Procedure for Real Fluids,"., *AIAA Journal*, Vol. 45, No. 10, pp2422-2428, October 2007

[5] Campbell, B.T., Davis, R.L., "A Quasi-1D Unsteady Flow Solver Module for Rocket Engine and Propulsion System Simulations," *ASME Journal of Fluids Engineering*, Vol. 131, No. 2, 2009.

[6] Churchill, S.W., "Friction-Factor Equation Spans all Fluid-Flow Regimes," *Chemical Engineering*, Vol. 84 No. 24, November 1977, pp.91-92.

[7] Cuffe, J. P. B, "Design Studies of RL10 Derivatives: Final Report Volume II Engine Design Characteristics," NASA Marshall Space Flight Center, December 1973.

[8] Cook, R.T., and Coffey, G.A., "Space Shuttle Orbiter Engine Main combustion Chamber Cooling and Life", Rocketdyne Division/Rockwell International, AIAA/SAE 9th Propulsion Conference, AIAA-73-1310, 1973.

[9] Davis, Roger L. Private discussions. September 2007 – June 2009.

[10] Esposito, J.J., and Zabora, R.F., "Thrust Chamber Life Prediction, Vol I. Mechanical and Physical Properties of High Performance Rocket Nozzle Materials," NASA CR-134806, 1975.

[11] Gordon, S. and McBride, B.J., "Computer Program for Calculation of Complex Chemical Equilibrium Compositions and Applications: I. Analysis", NASA Reference Publication 1311, October 1994.
<http://rocketworkbench.sourceforge.net/equil.phtml>

[12] Huzel, D.K., Huang, D.H., "Modern Engineering for Design of Liquid-Propellant Rocket Engines," AIAA, Washington, DC, 1992.

[13] Hyde, J.C., and Gill, G.S., "Liquid Rocket Engine Nozzles," NASA SP-8120, July 1976.

[14]Incropera, F.P., DeWitt, D.P., "Introduction to Heat Transfer," 4th Ed., John Wiley & Sons, Inc., New York, 2002.

[15]Klem, Mark D., Smith, Timothy D., "Propulsion and Cryogenics Advanced Development (PCAD) Project Propulsion Technologies for the Lunar Lander," Space Technology & Applications International Forum, Albuquerque, NM, February 2008.

[16]Kruger, R., Curren, A., "Some Factors Influencing Heat Transfer to Liquid-Propellant Rocket-Thrust-Chamber Coolant Channels," NASA TN D-3671, 1966.

[17] Mattingly, Jack D., "Elements of Gas Turbine Propulsion," AIAA, Virginia, 2005.

[18] NIST Database 23: NIST REFPROP, Reference Fluid Properties, Software Package, Ver. 7.0, National Institute of Standards and Technology, Boulder, CO.

[19]Shoenman, L., "Low-Thrust Isp Sensitivity Study", NASA CR-165621, Aerojet, 1982.

[20]Schuff, R., Maier, M., Sidiy, O., Ulrich, C., Fugger, S., "Integrated Modeling & Analysis for a LOX/Methane Expander Cycle Engine Focusing on Regenerative Cooling Design," Purdue University, West Lafayette, IN, December 2005.

[21] Schuff, R., Maier, M., Sidiy, O., Ulrich, C., Fugger, S., "Integrated Modeling and Analysis for a LOX/Methane Expander Cycle Engine: Focusing on Regenerative Cooling Jacket Design," AIAA 2006-4534, 42nd Jet Propulsion Conference & Exhibit, Sacramento, CA, 2006.

[22] Sutton, George P. and Biblarz, Oscar, "Rocket Propulsion Elements," 7th Ed., John Wiley & Sons, Inc., New York, 2001.

[23] Wadel, Mary F., "Comparison of High Aspect Ratio Cooling Channel Designs for a Rocket Combustion Chamber with Development of an Optimized Design," NASA TM 1998-206313, 1998.

[24] Zucrow, M.J., Hoffman, J.D., "Gas Dynamics", Vol. I, John Wiley & Sons, New York, 1976.

[25] Zucrow, M.J., Hoffman, J.D., "Gas Dynamics", Vol. II, *Multidimensional Flow*, (Reprint) Robert E. Krieger Publishing Company, Malabar, Florida, 1977